



DISSERTAÇÃO DE MESTRADO

**STUDIES ON FATIGUE OF TWO CONTACTING WIRES OF
OVERHEAD CONDUCTORS: EXPERIMENTS AND
MODELING**

Por,

PEDRO HENRIQUE CORREA ROCHA

Brasília, 30 de janeiro de 2019

UNIVERSIDADE DE BRASÍLIA

FACULDADE DE TECNOLOGIA
DEPARTAMENTO DE ENGENHARIA MECÂNICA

UNIVERSIDADE DE BRASÍLIA
Faculdade de Tecnologia
Departamento de Engenharia Mecânica

**STUDIES ON FATIGUE OF TWO CONTACTING
WIRES OF OVERHEAD CONDUCTORS:
EXPERIMENTS AND MODELING**

PEDRO HENRIQUE CORREA ROCHA

DISSERTAÇÃO DE MESTRADO SUBMETIDA AO DEPARTAMENTO DE ENGENHARIA MECÂNICA DA FACULDADE DE TECNOLOGIA DA UNIVERSIDADE DE BRASÍLIA, COMO PARTE DOS REQUISITOS NECESSÁRIOS PARA A OBTENÇÃO DO GRAU DE MESTRE EM CIÊNCIAS MECÂNICAS.

APROVADA POR:

Prof. Fábio Comes de Castro, D.Sc. (ENM/UnB)
(Orientador)

Prof. José Alexander Araújo, D.Phil. (ENM/UnB)
(Coorientador)

Prof. Jorge Luiz de Almeida Ferreira, D.Sc. (ENM/UnB)
(Examinador Interno)

Prof. Luís Augusto Conte Mendes Veloso, D.Sc. (ENM/UnB)
(Examinador Externo)

Brasília/DF, 30 de janeiro de 2019.

FICHA CATALOGRÁFICA

ROCHA, PEDRO HENRIQUE CORREA

Studies on fatigue of two contacting wires of overhead conductors: experiments and modeling.

[Distrito Federal] 2019.

xi, 52 p., 210 x 297 mm (ENM/FT/UnB, Mestre, Ciências Mecânicas, 2019)

Dissertação de mestrado – Universidade de Brasília.

Faculdade de Tecnologia.

Departamento de Engenharia Mecânica.

- | | |
|----------------------------|----------------------|
| 1. Overhead conductor | 2. Aluminum wire |
| 3. Fatigue life prediction | 4. Contact mechanics |

REFERÊNCIA BIBLIOGRÁFICA

ROCHA, P. H. C., (2019) Studies on fatigue of two contacting wires of overhead conductors: experiments and modeling. Dissertação de mestrado, Publicação ENM-DM 303/2019, Departamento de Engenharia Mecânica, Universidade de Brasília, DF, 63 p.

CESSÃO DE DIREITOS

AUTOR: Pedro Henrique Correa Rocha.

TÍTULO: Studies on fatigue of two contacting wires of overhead conductors: experiments and modeling.

GRAU: Mestre

ANO: 2019

É concedida à Universidade de Brasília permissão para reproduzir cópias desta dissertação de mestrado e para emprestar ou vender tais cópias somente para propósitos acadêmicos e científicos. O autor reserva outros direitos de publicação e nenhuma parte dessa dissertação de mestrado pode ser reproduzida sem autorização por escrito do autor.

Pedro Henrique Correa Rocha
Quadra 6 Conjunto A Casa 24
73025-061 Sobradinho – DF – Brasil.

Agradecimentos

Agradeço ao orientador deste trabalho e amigo Professor Fábio Comes de Castro pela exemplar orientação, paciência, suporte e confiança no trabalho desenvolvido ao longo destes dois anos de mestrado. Agradeço também o Professor José Alexander Araújo pelo apoio e incentivo dado ao desenvolvimento deste trabalho.

Agradeço aos amigos e parceiros de trabalho do Grupo de Fadiga, Fratura e Materiais. Em especial, agradeço aos amigos Remy Badibanga, Thiago Barbosa e Ricardo Lenon por toda a contribuição intelectual e técnica no desenvolvimento do trabalho; aos queridos amigos Guilherme Ferreira, Raniere Neves, Felipe Canut, Cainã de Barros, Leonel Morales, Vinicius Silva, Lucas Machado e Ian Matos não apenas pelos bons momentos de descontração, mas também pela de troca de ideias e experiências ao longo deste período de trabalho. Também agradeço aos queridos amigos José Monroy, Gabriel Juvenal, Rafael Cardoso, Pedro Machado, André Pinto, Lucas Mangas, Maurício González, Lucas Carneiro e Erick Vieira pelos bons momentos de conversa e discussões sobre os mais diversos assuntos. Agradecimento especial aos queridos amigos Remy Badibanga, José Monroy e Maurício González pelo fornecimento de alguns dos dados experimentais utilizados neste trabalho.

Por fim, Agradeço aos meus pais Elaine, Edilson e Luis por todo apoio, orientação e carinhosa motivação e que me deram ao longo desta jornada. Também agradeço aos meus irmãos Fernanda, Luis Guyllherme e João Marcos pela companhia e amizade de longa data que temos. Agradeço ao meu amigo Pedro Vinicius que ao longo de todos esses anos sempre esteve por perto e disponível para nossas agradáveis discussões e conversas sobre a vida. Finalmente, agradeço a Vitória Régia por todo amor, compreensão, companheirismo, carinho e incentivo que me foi dado ao longo destes anos.

Abstract

Under wind induced vibrations, overhead conductors are subjected to fatigue damage process. Usually wire ruptures are found close to regions where the conductor movement is restrained (e.g. at suspension clamps and dampers). In fact, fatigue failures on overhead conductors take place at the local (wire) scale, in the contact region between wires, or between outer layer wires and clamp. Therefore, an understanding of local contact interactions may lead to a better comprehension of the global fatigue behavior of overhead conductors. The aim of this thesis is to present contributions on fatigue of contacting wires of overhead conductors. Thus, this work is divided into two parts. First, a fatigue life prediction model for two contacting wires of an overhead conductor is developed. To account for the high stress gradient beneath the contact surface, an average of the stress distribution in a damage zone is considered. The characteristic length of the damage zone is determined by fitting the model to test data from sharply notched specimens. The evaluation of the fatigue model was carried out using wires made of 1350-H19 aluminum alloy, which were taken from the ACSR Ibis 397.5 MCM conductor. Fatigue test data of two contacting wires were obtained for normal loads equal to 250 N and 500 N. The crossing angle of all tests was 29° , which is the angle that was observed between the aluminum wires layers of the Ibis conductor. To calibrate the model, test data of plain wires, circumferentially V-notched wires, and wires with transverse hole under fully reversed axial loading were obtained. Most of the predicted lives were within factor-of-three boundaries, which is a range similar to the scatter of the calibration data. Predicted lives were not significantly altered by the data set used to calibrate the fatigue model. On the second part, it is presented an experimental-numerical methodology to determine the loading conditions of two contacting wires of the AAAC 900 MCM conductor. As a first step, 9 conductors previously tested at the resonance fatigue test bench of the University of Brasilia were examined to identify the zones near the clamping region where the wire breakages occurred. Most of the breakages were detected at the upper part of the external layer of the conductor. Cyclic and static stresses were calculated from strain measurements on wires located at the critical region of the cable on additional tests. The measurements revealed that wires on the critical region are subjected to tensile loads up to 4.57 times the load on wires located at a free span of the cable. Measurements obtained from the cyclic test showed similar values to the Poffenberger–Swart model for amplitude stress. To determine the normal contact loads between two contacting wires, elastic-plastic finite element simulations were carried out. The simulation results were compared to marks found in the critical region of the cable. The contact marks' loads vary between 100 N and 1290 N on the analyzed region.

Resumo

Cabos condutores de energia estão sujeitos ao processo de fadiga quando submetidos a vibrações induzidas pelo vento. As falhas por fadiga são encontradas normalmente em fios localizados em regiões onde o movimento do cabo é restringido como, por exemplo, em grampos de suspensão e amortecedores de vibração. Mais especificamente, as falhas por fadiga em cabos condutores de energia ocorrem na região de contato entre fios ou entre fios da camada externa e o grampo de suspensão. Portanto, entender interações de contato locais pode resultar em uma melhor compreensão do comportamento à fadiga do cabo. O objetivo deste trabalho é apresentar contribuições a respeito do processo de fadiga associado ao contato entre fios de cabos condutores de energia. O trabalho é apresentado em duas partes. Na primeira parte, um modelo para predição de vida de dois fios de cabos condutores de energia em contato sob condições de fadiga é desenvolvido. Para levar em consideração o alto gradiente de tensão logo abaixo do contato, é feita uma média da distribuição de tensão na zona de dano do fio. O tamanho característico da zona de dano é determinado pelo ajuste do modelo a dados experimentais de corpos de prova contendo entalhes afiados. A avaliação do modelo de fadiga foi feita utilizando fios da liga de alumínio 1350-H19, retirados do cabo CAA Ibis 397.5 MCM. Dados de fadiga dos fios em contato foram obtidos para cargas de contato normais iguais a 250 N e 500 N. O ângulo de inclinação entre fios era 29° , similar ao ângulo entre fios de camadas adjacentes do cabo Ibis. Para calibrar o modelo, dados experimentais de fios lisos, fios com entalhe circunferencial em V e fios com furo transversal sob carregamentos totalmente alternados foram obtidos. A maior parte das vidas previstas estão dentro do fator 3, similar a faixa de dispersão dos dados de calibração do modelo. Na segunda parte do trabalho, é apresentada uma metodologia numérico-experimental para determinar condições de carregamento de fios em contato do cabo CAL 900 MCM. Primeiramente, 9 condutores previamente testados na bancada de ensaios de cabos de transmissão de energia da Universidade de Brasília foram examinados e regiões onde as rupturas ocorreram foram identificadas. A maior parte das falhas foram detectadas na região superior da camada mais externa do cabo, próxima ao grampo de suspensão. Tensões cíclicas e estáticas em fios da região crítica de falha do cabo foram calculadas a partir de medidas obtidas de *strain gages* em ensaios adicionais no cabo. Identificou-se que fios na região de falha do cabo podem estar submetidos a carregamentos estáticos até 4,57 vezes maior do que na região de vão livre do cabo, enquanto que a amplitude de tensão encontrada durante o ensaio cíclico é similar ao previsto pelo modelo de Poffenberger–Swart. Para determinar a carga normal de contato entre os fios, foram feitas simulações elasto-plásticas do contato normal entre os fios utilizando o método de elementos finitos. Os resultados das simulações foram comparados às marcas da região crítica do cabo. Constatou-se que as cargas de contato podem variar entre 100 N e 1290 N na região analisada.

Contents

1	Introduction	1
1.1	Motivation	1
1.2	Objectives	1
1.3	Outline of the work	2
2	Fatigue of two contacting wires of the ACSR Ibis 397.5 MCM conductor: Experiments and life prediction.....	3
2.1	Introduction	3
2.2	Experimental work	4
2.3	Fatigue model.....	11
2.4	Stress analysis	14
2.5	Results and discussion.....	16
2.6	Conclusions	19
3	Experimental–numerical methodology for the determination of the loading conditions of two contacting wires of the AAAC 900 MCM conductor	21
3.1	Introduction	21
3.2	Observation of the fatigue-critical region of the AAAC 900 MCM conductor	22
3.3	Estimation of the loading conditions of two contacting wires of the fatigue-critical region of the conductor	28
3.4	Two contacting wires – preliminary tests	46
3.5	Conclusions and future work	47
	References	49

List of Figures

Fig. 2.1. Specimens used to calibrate the fatigue life model: (a) plain wire, (b) circumferentially V-notched wire, and (c) wire with transverse hole. (All dimensions in mm)	6
Fig. 2.2. Stress amplitude versus fatigue life for fully reversed axial loading: (a) plain wire, (b) circumferentially V-notched wire, and (c) wire with transverse hole.	8
Fig. 2.3. Experimental apparatus for fatigue testing of two contacting wires.....	9
Fig. 2.4. Maximum stress versus fatigue life for the tests conducted on two contacting wires: (a) $P = 250\text{ N}$; (b) $P = 500\text{ N}$	11
Fig. 2.5. Schematic of the fatigue damage zone near a notch.	12
Fig. 2.6 FE meshes: (a) circumferentially V-notched wire; (b) wire with transverse hole.....	15
Fig. 2.7. FE model of the contacting wires: (a) boundary conditions; (b) mesh; (c) loading history.....	15
Fig. 2.8. Correlation between the characteristic length and the number of cycles to failure obtained using test data from V-notched wires and wires with transverse hole.	17
Fig. 2.9. Observed life versus predicted life for the wire-wire tests. Fatigue model calibrated using test data from (a) V-notched wires and (b) wires with transverse hole.....	19
Fig. 3.1. (a) Schematic of the resonance fatigue test benches of the Laboratory of Fatigue and Structural Integrity of Overhead Conductors of the University of Brasilia, and (b) Conductor assembled with suspension clamp.....	23
Fig. 3.2. S-N curve for AAAC 900 MCM conductor static tensile load of 26.3 kN.	25
Fig. 3.3. Terminology for the identification of the location of wire breaks within the cross section of the AAAC 900 MCM conductor.	26
Fig. 3.4. Distribution of wire breaks within the cross section of the conductor for different stress amplitudes.	26
Fig. 3.5. (a) Coordinate distance from keeper edge of the conductor/clamp assembly; (b) Distances of wire breaks observed at the external layer of the upper part of the conductor....	27
Fig. 3.6. Strain gages located at the fatigue-critical region, in detail: keeper edge (KE) location, region diametrically opposed to the last point of contact (LPC) between conductor and clamp, and location 20 mm ahead of KE.	31

Fig. 3.7. Static strain distribution on wires A, B and C for a mean tensile load equal to 26.3 kN.	32
Fig. 3.8. Strain gauges fixed close to the keeper edge (1, 2 and 3) and on the region diametrically opposed to the LPC of the cable/clamp (4, 5 and 6).	34
Fig. 3.9. FE mesh of the contacting wires: (a) global model; (b) fine mesh partitions on the contact region.	36
Fig. 3.10. Stress-strain curve of AA 6201-T81 wire extracted from AAAC 900 MCM conductor.	37
Fig. 3.11. Script used to determine the normal contact load between two wires.	38
Fig. 3.12. Experimental apparatus for fatigue testing of two contacting wires.	39
Fig. 3.13. Major vs. minor semi-axis measurements for different contact load levels.	40
Fig. 3.14. Samples of the three upper wires taken to microscopy analyses, in detail fretting marks between the samples and the inner layer of the AAAC 900 conductor.	41
Fig. 3.15. Observed and numerical marks for contact load prediction: (a) contact mark 1, (b) contact mark 2, (c) contact mark 3, (d) contact mark 4, (e) contact mark 5, (f) contact mark 6, (g) contact mark 7 and (h) contact mark 8. (refer to Fig. 3.14).	45
Fig. 3.16. Normal contact load prediction for marks from critical region of the cable.	45

List of Tables

Table 2.1. Summary of the fatigue tests of plain wires.....	6
Table 2.2. Summary of the fatigue tests of circumferentially V-notched wires.	7
Table 2.3. Summary of the fatigue tests of wires with transverse circular hole.	7
Table 2.4. Summary of the fatigue tests of two contacting wires crossed at an angle of 29°..	10
Table 3.1. Strains obtained from strain gages attached at the critical region of the AAAC 900 MCM conductor, and estimated values of the mean stress experienced by the wires.	32
Table 3.2. Strain amplitudes obtained from strain gages attached at the critical region of the AAAC 900 MCM conductor, and estimated values of the stress experienced by the wires. ..	35
Table 3.3. Summary of the fatigue tests of two contacting wires crossed at an angle of 29°..	46

Nomenclature

A_{wire}	cross-sectional area of an aluminum wire
a	major semi-axis length of the elliptical contact mark
b	minor semi-axis length of the elliptical contact mark
D	diameter of the specimen
d	diameter of an aluminum wire of the outermost layer of the conductor
d_h	diameter of the transverse hole
d_{min}	minimum diameter of the specimen
E_a	Young's modulus of an aluminum wire of the outermost layer of the conductor
EI	minimum flexural stiffness of the conductor
F_a	axial load amplitude on a wire
F_m	mean axial load
L	characteristic length of the damage zone
N_f	number of cycles to failure
P	normal contact load
R	load ratio
r	V-notch radius
SWT	Smith-Watson-Topper parameter
S_a	nominal stress amplitude based on the net cross section of a wire
S_m	nominal mean stress based on the net cross section of a wire
V	damage zone volume
ε_a	strain amplitude
ε_m	mean traction strain
φ	V-notch opening angle
σ_a	stress amplitude obtained from the Poffenberger–Swart formula
σ_m	mean stress
$\hat{\sigma}$	stress tensor
$\langle \rangle$	Macaulay brackets

1 Introduction

1.1 Motivation

Fatigue damage is one of the main concerns about structural integrity of overhead conductors. The cause of the fatigue process is usually associated to aeolian vibration of the conductor. The alternating deflection of the conductor causes fatigue failures in regions where the motion of the cable is restrained (e.g. at suspension clamps or support locations). Experimental observations indicate that fretting damage due to minute relative displacement between wires or between conductor and suspension clamp is associated to rupture of wires (Cardou et al., 1992, Zhou et al., 1994a).

Over the years tests in overhead conductors have been performed to better understand the global mechanical behavior of such components. These studies revealed that features such as mean tensile load, bending stress amplitude, suspension clamp geometry, clamping force and type of conductor have been identified as some of the important parameters that affects fatigue performance of overhead conductors (Cardou et al., 1993, Fadel et al., 2012, Baumann and Novak, 2017).

In fact, fatigue failures on overhead conductors take place at the local (wire) scale. More specifically, in the contact region between wires, or between outer layer wires and clamp. Therefore, an understanding of local mechanical interactions of the wire-wire, or wire-clamp may lead to a better assessment of fatigue behavior of overhead conductors.

1.2 Objectives

This research work presents numerical and experimental investigations about the contact between wires under cyclic loads. The study is divided into two parts. On the first part, a fatigue life model for contacting wires subjected to cyclic loads is presented. The major feature of the model is the use of an average stress over a fatigue damage zone to account for the high stress gradients beneath the contact surface. The multiaxial version of the Smith-Watson-Topper parameter based on critical plane concept is investigated on the proposed methodology. The calibration of the model

is carried out by fitting uniaxial test data from plain and notched wires. Life predictions using two different types of notches to calibrate the fatigue model are compared. Predicted lives were evaluated using fatigue test data of two contacting AA1350-H19 wires taken from the ACSR Ibis 397.5 MCM conductor. On the second part of the work, a methodology is proposed to determine local loading conditions of wires of a AAAC 900 MCM conductor. The study is done based on critical region of failure of the conductor. An examination of previously tested conductors is done to identify the location of this critical region. Strain measurements obtained from static and dynamic tests carried out on this cable are used on loading conditions determination. A finite element model of the contact between two wires is used on determination of contact load between two strands of adjacent layers.

1.3 Outline of the work

This work is organized into three chapters. The Chapter 1 presents the motivation and the main objectives and features of the work. Chapter 2 describes the fatigue model used to make life prediction of two contacting wires. Chapter 3 describes the methodology to determine the loading conditions of wires located on a typical region of failure of a conductor. Chapters 2 and 3 are structured as scientific articles and are intended to be published in scientific journals.

2 Fatigue of two contacting wires of the ACSR Ibis 397.5 MCM conductor: Experiments and life prediction

2.1 Introduction

Fatigue of wires is the most common type of failure encountered in overhead conductors and may threaten the safe and stable operation of the transmission line. Fatigue failure of wires typically occurs in regions where the movement of the conductor is restrained, such as at suspension clamps (Cardou et al., 1992, Zhou et al., 1994a). Field and laboratory observations of broken wires have clearly indicated fretting damage due to the minute relative movements between conductor wires or between conductor and suspension clamp (Azevedo and Cescon, 2002; Zhou et al., 1996, EPRI, 1979, Fadel et al., 2012).

Test benches have been developed over the past decades to understand the mechanical response and fatigue behavior of overhead conductors (Cardou et al., 1990; Cloutier et al., 2006; Azevedo et al., 2009; Lévesque et al., 2010; Fadel et al., 2012; Baumann and Novak, 2017). Among the major factors that affect the performance of the conductors are the bending stress amplitude, mean tensile stress, suspension clamp geometry, clamping force, and type of conductor. In parallel to these experimental studies, efforts have also been directed towards the development of finite element models for the stress analysis of the contact between a suspension clamp and a single wire (Lévesque et al., 2011a), of multi-layered wire strands (Lalonde et al., 2017), and of the conductor-clamp assembly (Qi, 2013; Lalonde et al., 2018).

Fatigue tests of overhead conductors are essential to understand their behavior at the structural level. However, such tests are expensive and technologically difficult to perform. Furthermore, a realistic numerical simulation of a multi-layer conductor or of a conductor-suspension clamp system is extremely complex and time-consuming because of the nonlinear effects introduced by the hundreds of contact zones, plasticity and wear. Fatigue failure of conductors, as a matter of fact, takes place at the local (wire) scale by damage accumulation in the contact region between wires,

or between outer layer wires and clamp. Therefore, an understanding of the wire-wire, or wire-clamp, contact fatigue problem may lead to a better evaluation of the conductor fatigue performance.

Despite the importance of understanding the single contact interaction between wires, or between wire and clamp surface, few studies have been done on this topic. Zhou et al. (1995) carried out fretting fatigue tests on single wire in contact with the surface of a suspension clamp. It was found that features such as fretting zone size and number of cycles to crack initiation were similar to the ones observed on full-scale tests. Lévesque et al. (2011a) performed an elastic-plastic finite element analysis of the contact interaction between a wire and the bed of a suspension clamp, and a simple fatigue analysis was done using a damage parameter proposed by Ruiz et al. (1984). Lévesque and Légeron (2011a) investigated the effect of mean tension on interwire contacts in overhead conductors using elastic-plastic finite element simulation, concluding that the static tension has little influence on the contact stresses.

Fatigue analysis of overhead conductors has relied on traditional S-N curves. To the best of the authors' knowledge, the use of modern fatigue analysis tools to predict the life of contacting wires of overhead conductors has not yet been investigated. This work presents a fatigue life model for contacting wires subjected to cyclic loads. The major feature of the model is the use of an average stress over a fatigue damage zone to account for the high stress gradients beneath the contact surface. The calibration of the model is carried out by fitting uniaxial test data from plain and notched wires. Life predictions were evaluated using fatigue test data of two contacting AA1350-H19 wires taken from the ACSR Ibis 397.5 MCM conductor.

2.2 Experimental work

The material investigated in this work is the 1350-H19 aluminum alloy used to manufacture the wires of overhead conductors. Typically, AA1350-H19 has a modulus of elasticity of 69 GPa, yield stress of 165 MPa, and ultimate tensile strength of 185 MPa (Kaufman, 2000). The experimental program consisted of fatigue tests on plain and notched wires under axial loading,

which were used to determine the constants of the fatigue life prediction methodology. In addition, fatigue tests on two contacting wires were carried out to evaluate the life estimates of the proposed methodology.

Figure 2.1 shows the geometry and dimensions of the plain wire, circumferentially V-notched wire, and wire with transverse hole. These specimens were manufactured from 3.38 mm-diameter wires of the ACSR Tern overhead conductor. The reason for choosing sharply notched specimens is that they produce high stress gradients near the notch, which are required for the characterization of the size of the fatigue process zone (Taylor, 1999; Susmel and Taylor, 2007). The fatigue tests were performed using a servo-hydraulic axial testing machine (MTS Landmark) equipped with a load cell with a capacity of 5 kN. The specimens were subjected to fully reversed axial loading and the loading frequency was chosen between 10 Hz and 15 Hz. Failure was defined as the complete rupture of a specimen and run-out was set at 5×10^6 cycles. In most cases, the fatigue tests at a given loading condition were replicated three times. A summary of the fatigue test data obtained from the plain and notched specimens is presented in Tables 2.1–3. The stress quantities in these tables are nominal values based on the net cross-sectional area. The nominal stress amplitude–fatigue life plot for each data set is shown in Fig. 2.2. A data point with a horizontal arrow denotes a run-out test. The dashed lines in Fig. 2.2a and b are factor-of-three boundaries, and the ones in Fig. 2.2c are factor-of-two boundaries. The higher level of dispersion found on fatigue data of plane and circumferentially V-notched wire in comparison with specimens containing transverse hole may be associated to a higher dimensional variability of the first two types of specimens due to manufacture process.

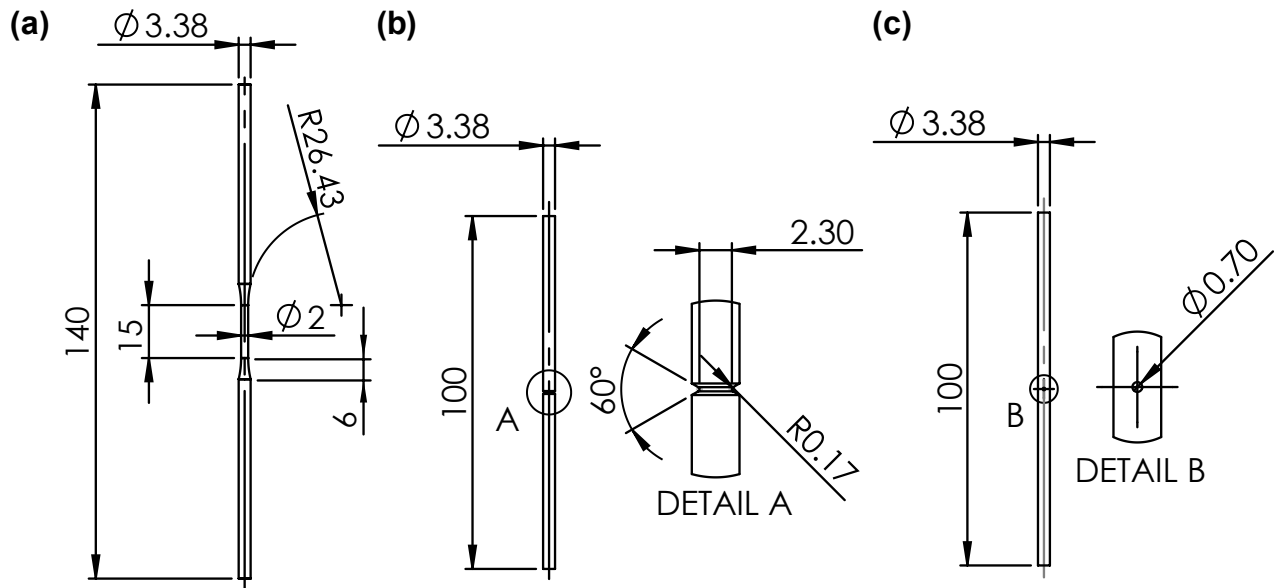


Fig. 2.1. Specimens used to calibrate the fatigue life model: (a) plain wire, (b) circumferentially V-notched wire, and (c) wire with transverse hole. (All dimensions in mm)

Table 2.1. Summary of the fatigue tests of plain wires.

Specimen ID	D [mm]	d_{\min} [mm]	F_a [N]	S_a [MPa]	N_f [cycles]
1350U1	3.38	2.00	314	100.00	84,356
1350U2	3.38	2.00	314	100.00	109,834
1350U3	3.38	2.00	314	100.00	123,242
1350U4	3.38	2.00	283	90.00	473,045
1350U5	3.38	2.00	283	90.00	547,421
1350U6	3.38	2.00	283	90.00	1,257,270
1350U7	3.38	2.00	251	80.00	2,150,257
1350U8	3.38	2.00	251	80.00	2,713,742
1350U9	3.38	2.00	251	80.00	3,876,713

Table 2.2. Summary of the fatigue tests of circumferentially V-notched wires.

Specimen ID	D [mm]	d_{\min} [mm]	r [mm]	φ [°]	F_a [N]	S_a [MPa]	N_f [cycles]
1350N17	3.45	2.42	0.17	61	346	75.00	187,247
1350N11	3.40	2.44	0.18	60	352	75.00	394,000
1350N15	3.44	2.55	0.18	64	372	72.69	261,607
1350N30	3.42	2.37	0.17	61	308	70.00	433,502
1350N1	3.41	2.41	0.15	62	319	70.00	467,836
1350N28	3.44	2.39	0.17	60	292	65.00	545,728
1350N24	3.38	2.31	0.17	62	272	65.00	953,328
1350N22	3.45	2.43	0.17	61	281	60.55	2,839,057
1350N19	3.43	2.57	0.17	63	311	60.00	758,576
1350N16	3.45	2.58	0.17	63	314	60.00	1,080,320
1350N27	3.43	2.38	0.17	60	245	55.00	929,024
1350N20	3.44	2.48	0.17	59	267	55.00	1,580,039
1350N25	3.43	2.51	0.17	61	273	55.00	2,624,388
1350N10	3.44	2.47	0.17	62	239	50.00	3,157,871
1350N13	3.40	2.33	0.17	59	213	50.00	>5,160,068
1350N23	3.44	2.50	0.17	61	246	50.00	>6,509,908
1350N7	3.39	2.44	0.17	62	210	45.00	>5,109,252
1350N18	3.38	2.42	0.18	64	207	45.00	>6,337,954

Table 2.3. Summary of the fatigue tests of wires with transverse circular hole.

Specimen ID	D [mm]	d_h [mm]	F_a [N]	S_a [MPa]	N_f [cycles]
1350H3	3.38	0.70	495	75.00	87,242
1350H4	3.39	0.72	459	70.00	131,306
1350H7	3.38	0.73	423	65.00	590,395
1350H5	3.38	0.72	393	60.00	743,253
1350H13	3.39	0.72	393	60.00	796,499
1350H12	3.46	0.73	377	55.00	794,089
1350H2	3.41	0.77	357	55.00	831,325
1350H9	3.32	0.69	317	50.00	1,541,990
1350H11	3.38	0.73	325	50.00	1,892,158
1350H1	3.47	0.70	316	45.00	2,545,480
1350H10	3.38	0.75	290	45.00	>5,014,845
1350H8	3.29	0.69	249	40.00	>5,240,661

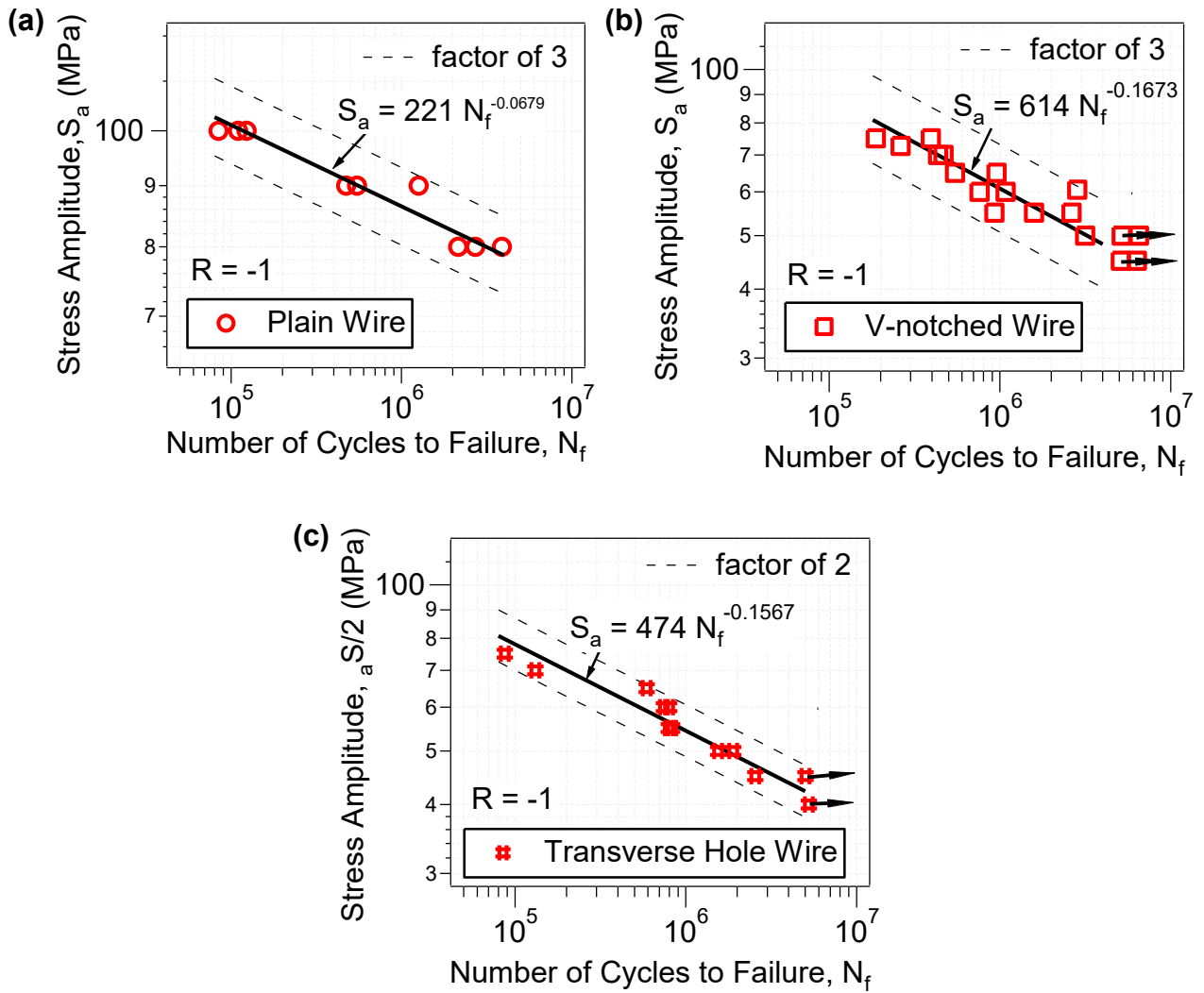


Fig. 2.2. Stress amplitude versus fatigue life for fully reversed axial loading: (a) plain wire, (b) circumferentially V-notched wire, and (c) wire with transverse hole.

The fatigue tests on two contacting wires were performed using the experimental apparatus shown in Fig. 2.3. The apparatus consists of a lower hydraulic actuator which applies a remote cyclic loading to the specimen (vertical wire) and an upper hydraulic actuator which allows the application of a tangential loading. Pneumatic actuators are used to apply a normal load to the pad (oblique wire) and a bearing, and a digital control system ensures that the normal load is kept at a fixed level. The apparatus allows to adjust the crossing angle of the two wires so as to reproduce the angle between wires of adjacent layers of an overhead conductor.

Wires with diameter of 3.14 mm taken from an ACSR Ibis 397.5 MCM conductor were tested. The crossing angle of all fatigue tests was chosen as 29° , which is the angle that was observed

between the aluminum wires layers of the Ibis conductor. The loading history of each fatigue test was defined as follows: a remote mean load, F_m , was applied to the vertical wire, which was followed by the application of a fixed normal load, P , to the oblique wire; then, the remote load was cycled with a constant amplitude, $\Delta F/2$. The ratio of minimum to maximum remote load was equal to 0.1, and the loading frequency was 10 Hz. In all tests, the displacement of the upper hydraulic actuator was kept fixed.

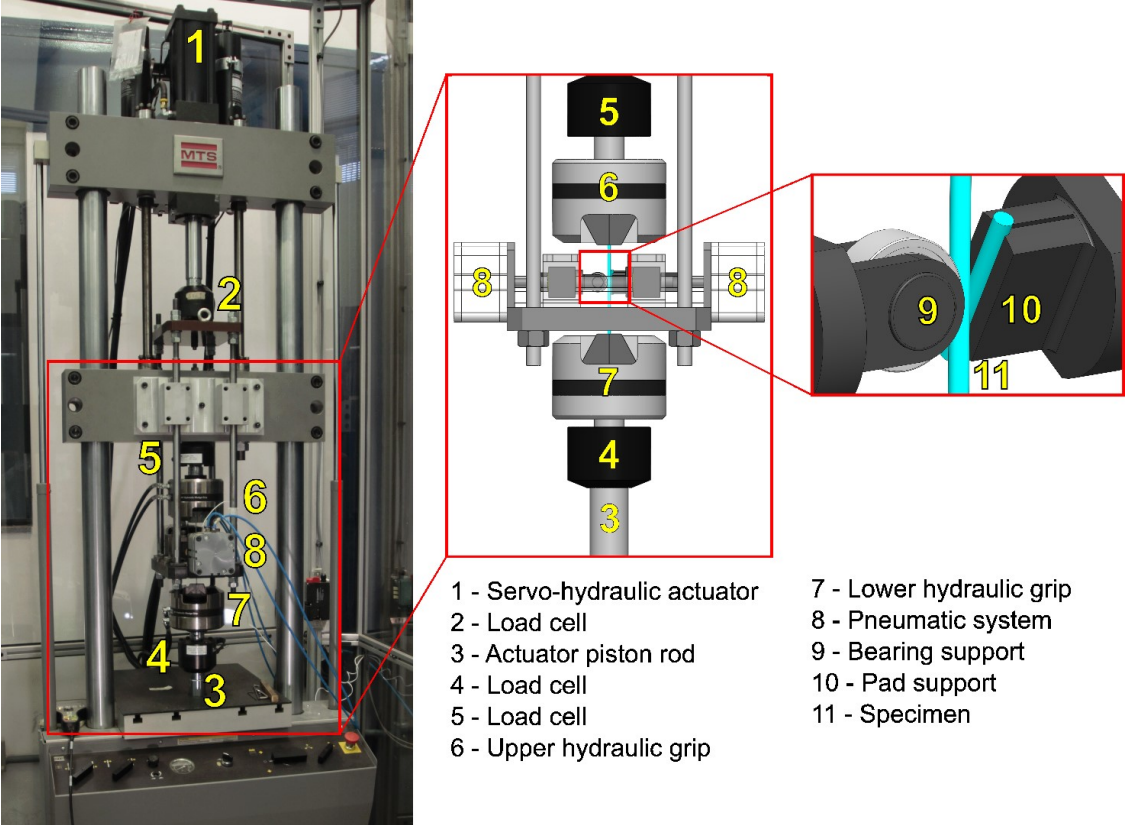


Fig. 2.3. Experimental apparatus for fatigue testing of two contacting wires.

The fatigue test data of two contacting wires are summarized in Table 2.4. Two data sets were obtained for normal loads equal to 250 N and 500 N. In most cases, the fatigue tests at a given loading condition were replicated three times. All specimens were tested to total separation into two parts. The maximum stress–fatigue life plot of each data set is shown in Fig. 2.4. The dashed lines in Fig. 2.4a are factor-of-three boundaries, and the ones in Fig. 2.4b and c are factor-of-two boundaries. The scatter of the fatigue lives of the wire-wire contact configuration is similar to that of the plain and notched specimens.

Table 2.4. Summary of the fatigue tests of two contacting wires crossed at an angle of 29°.

Specimen ID	D [mm]	P [N]	F_m [N]	$\Delta F/2$ [N]	S_m [MPa]	S_a [MPa]	N_f [cycles]
1350C94	3.14	250	554	453	71.50	58.50	122,717
1350C92	3.14	250	554	453	71.50	58.50	166,417
1350C93	3.14	250	554	453	71.50	58.50	255,336
1350C1	3.14	250	554	453	71.50	58.50	491,213
1350C82	3.14	250	511	418	66.00	54.00	451,267
1350C84	3.14	250	511	418	66.00	54.00	491,213
1350C83	3.14	250	511	418	66.00	54.00	517,525
1350C79	3.14	250	468	383	60.50	49.50	460,457
1350C80	3.14	250	468	383	60.50	49.50	974,159
1350C74	3.14	250	426	348	55.00	45.00	552,076
1350C89	3.14	250	426	348	55.00	45.00	632,997
1350C75	3.14	250	426	348	55.00	45.00	686,207
1350C73	3.14	250	426	348	55.00	45.00	831,909
1350C72	3.14	250	426	348	55.00	45.00	2,828,421
1350C68	3.14	500	511	418	66.00	54.00	217,865
1350C67	3.14	500	511	418	66.00	54.00	348,895
1350C30	3.14	500	511	418	66.00	54.00	590,099
1350C31	3.14	500	426	348	55.00	45.00	592,855
1350C27	3.14	500	426	348	55.00	45.00	848,192
1350C7	3.14	500	426	348	55.00	45.00	859,534
1350C33	3.14	500	426	348	55.00	45.00	929,227
1350C70	3.14	500	341	279	44.00	36.00	1,491,856
1350C105	3.14	500	341	279	44.00	36.00	2,275,383
1350C69	3.14	500	341	279	44.00	36.00	3,321,990
1350C32	3.14	500	341	279	44.00	36.00	3,382,328
1350C4	3.14	500	319	261	41.25	33.75	2,702,898
1350C6	3.14	500	319	261	41.25	33.75	4,815,976
1350C57	3.14	500	319	261	41.25	33.75	>7,233,660
1350C3	3.14	500	298	244	38.50	31.50	3,211,605
1350C2	3.14	500	298	244	38.50	31.50	3,482,397

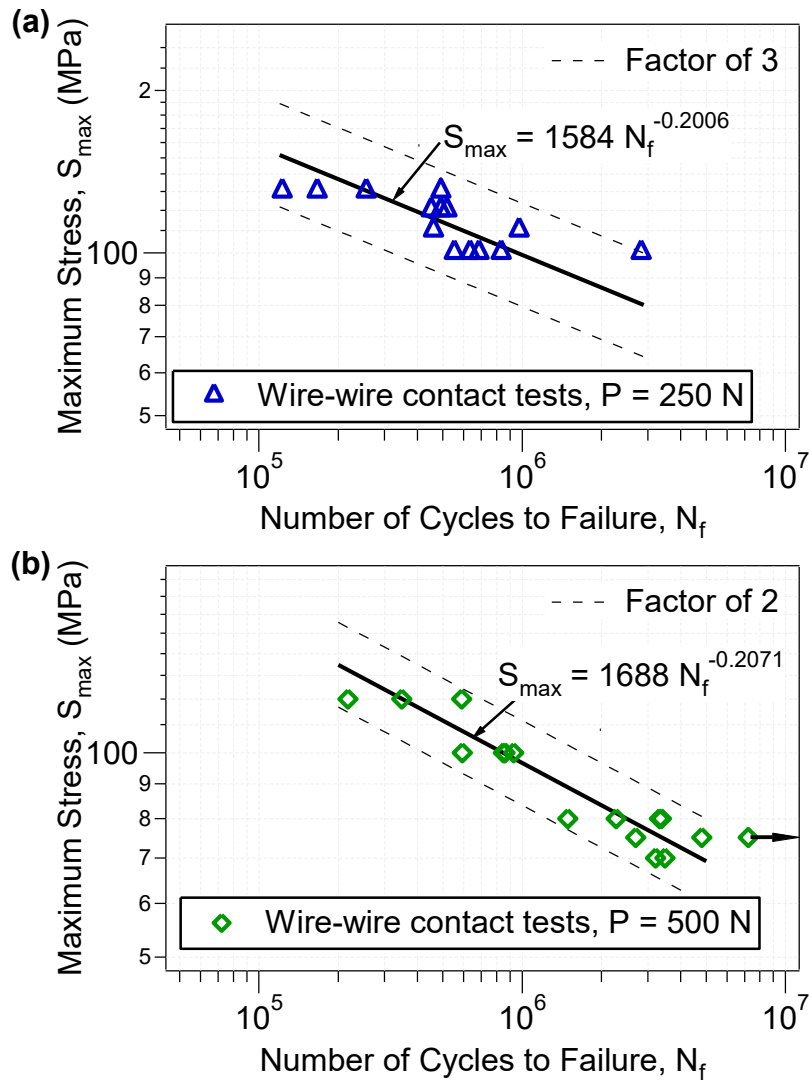


Fig. 2.4. Maximum stress versus fatigue life for the tests conducted on two contacting wires: (a) $P = 250$ N; (b) $P = 500$ N.

2.3 Fatigue model

The contact of two wires of an overhead conductor results in severe stress concentration and high stress gradients. Similar features are observed in sharp notches and, therefore, it might be possible to apply notch fatigue life prediction approaches to the fatigue analysis of two contacting wires. In the present work, the so-called Theory of Critical Distances (Taylor, 2007; Susmel, 2009) is evaluated using the AA1350-H19 wire-wire test data described in Section 2.2.

The Theory of Critical Distances (TCD) is based on the simple idea of using an average stress, instead of the stress at the hot-spot, to account for the stress gradient effect on fatigue life. The volume method is used in the present work, therefore the average stress is defined as

$$\sigma = \frac{1}{V} \int_V \hat{\sigma} dV \quad (2.1)$$

where V is the volume of the damage zone and $\hat{\sigma}$ is the stress tensor obtained from linear elastic stress analysis. The shape of the damage zone is a semi-sphere of radius L surrounding the hot-spot, as illustrated in Fig. 2.5.

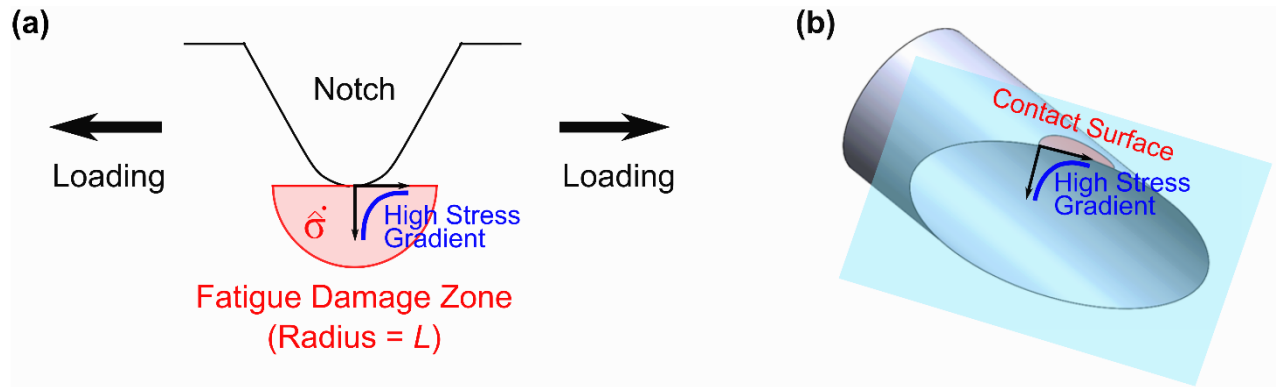


Fig. 2.5. Schematic of the fatigue damage zone near a notch.

To quantify the fatigue damage, the multiaxial version of the Smith, Watson and Topper (SWT) parameter based on the critical plane concept is adopted (Smith et al., 1970; Socie, 1987). The reason for choosing the SWT parameter was that it usually performs better for aluminum alloys than other fatigue parameters (Dowling et al., 2009). For a linear elastic stress-strain behavior, the SWT parameter can be written as

$$SWT = \sqrt{\frac{\Delta\sigma}{2} \langle \sigma_{n,max} \rangle} \quad (2.2)$$

where $\Delta\sigma/2$ is the stress amplitude, and $\sigma_{n,max}$ is the maximum stress in a loading cycle. The critical plane is defined as the material plane where the fatigue parameter is maximum. To calculate the fatigue parameter, the history of the average stress tensor defined in Eq. (2.1) is used as input data.

The symbols $\langle \rangle$ represent the Macaulay brackets defined as $\langle x \rangle = 0.5(x + |x|)$. The use of the Macaulay brackets ensures that no negative damage can be produced. The relationship between the fatigue parameter and the number of cycles to failure was described by a power-law function:

$$SWT = \alpha N_f^\beta \quad (2.3)$$

where α and β are constants obtained by best fitting test data from plain specimens.

The determination of the size of the fatigue damage zone is a crucial aspect of the TCD. In the early versions of the TCD, the so-called line and point methods developed by Neuber (1958) and Peterson (1959), the size of the damage zone (also known as critical distance) was determined using empirical expressions. Later, Taylor (1999) proposed a procedure to obtain the size of the damage zone based on fitting fatigue test data from specimens under high stress gradients (cracked or sharply notched specimens). Taylor's approach was limited to the prediction of the fatigue threshold condition. To extend the original approach to the prediction of fatigue lives, Susmel and Taylor (2007) assumed that the size of the damage zone is related to the number of cycles to failure according to a power-law relationship:

$$L = \gamma N_f^\delta \quad (2.4)$$

where γ and δ are constants determined by best fitting test data from specimens subjected to high stress gradients.

Eqs. (1)–(4) define the fatigue life of a component subjected to cyclic loading. To calculate the fatigue life, one must find the solution N_f of Eq. (2.3). In the presence of stress gradients, the left-hand side of Eq. (2.3) (SWT parameter) depends on the characteristic length of the damage process zone. Since the characteristic length is a function of the number of cycles to failure, an iterative algorithm is required to solve Eq. (2.3). This equation was solved in the present work by using the interval halving method.

2.4 Stress analysis

The first step to make fatigue life estimates based on the model described in Section 2.3 is to determine as accurately as possible the stress field in the critical region of a component. An appealing feature of the model is that the input stress data comes from a linear elastic stress analysis, which is simpler and faster to perform than a cyclic plastic analysis. This section presents the finite element (FE) model that was employed to obtain the stress field of the circumferentially V-notched wire, the wire with transverse hole, and the wire in contact with a crossed wire. The first two FE models provided the stress data required to calibrate the fatigue model, and the third FE model provided the stress data used to make the fatigue life predictions of the wire-wire contact configurations. All stress analyses were performed using the finite element software package Abaqus (2013).

The FE models of the circumferentially V-notched wire and wire with transverse hole were created using a solid cylinder of diameter of 3.38 mm. A Young's modulus of 68.9 GPa and Poisson's ratio of 0.33 were used as the elastic constants of the AA1350-H19. The FE mesh of the circumferentially V-notched wire is shown in Fig. 2.6a. For the bulk of the wire, a coarse non-structured mesh of ten-node quadratic tetrahedral elements (C3D10) was created. Near the notch root, a very fine mesh was required to compute the high stress gradients accurately. To accomplish this, a partition of eight-node linear brick elements with reduced integration (C3D8R) was created in a volume of approximately $1000 \times 2000 \times 1500 \mu\text{m}^3$. The characteristic size of an element in the partition was $20 \mu\text{m}$. The tie constraint option available in Abaqus was applied to the lateral and bottom surfaces of the partition to fuse together the brick and tetrahedral elements. The use of this technique allowed an easy control of the mesh size in the region of interest, i.e. the vicinity of the contact surface, and simplified the mesh design by eliminating the creation of an increasing level of refinement towards the region of interest. The mesh design for the wire with a transverse hole

followed a similar procedure, as shown in Fig. 2.6b. The volume of the partition was approximately $1500 \times 1500 \times 3380 \mu\text{m}^3$ and the characteristic element size was $30 \mu\text{m}$.

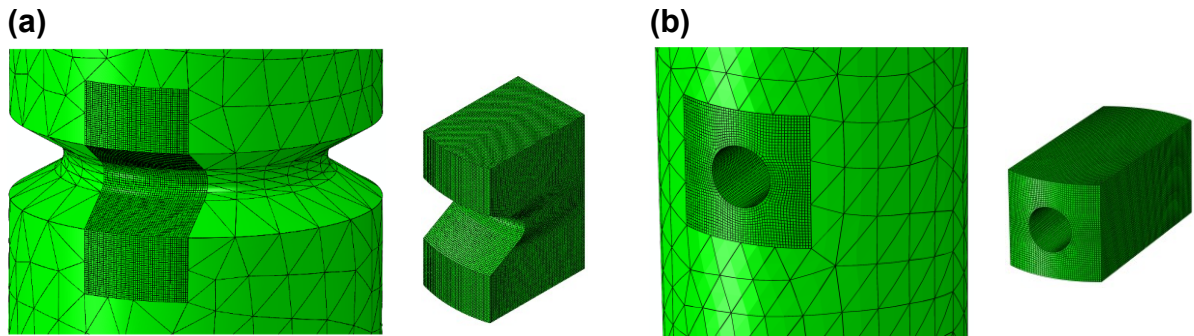


Fig. 2.6 FE meshes: (a) circumferentially V-notched wire; (b) wire with transverse hole.

Figure 2.7 shows the FE model of the contacting wires, which is composed of a vertical wire (specimen) positioned with its axis parallel to y-axis and an inclined wire (pad) crossed at an angle of 29° with respect to the specimen. Only half of the vertical wire was modeled to reduce the computation time. Both wires have a diameter of 3.14 mm to comply with the specification of the ACSR Ibis 397.5 MCM conductor. A linear elastic material model with Young's modulus of 68.9 GPa and Poisson's ratio of 0.33 was used to describe the constitutive behavior.

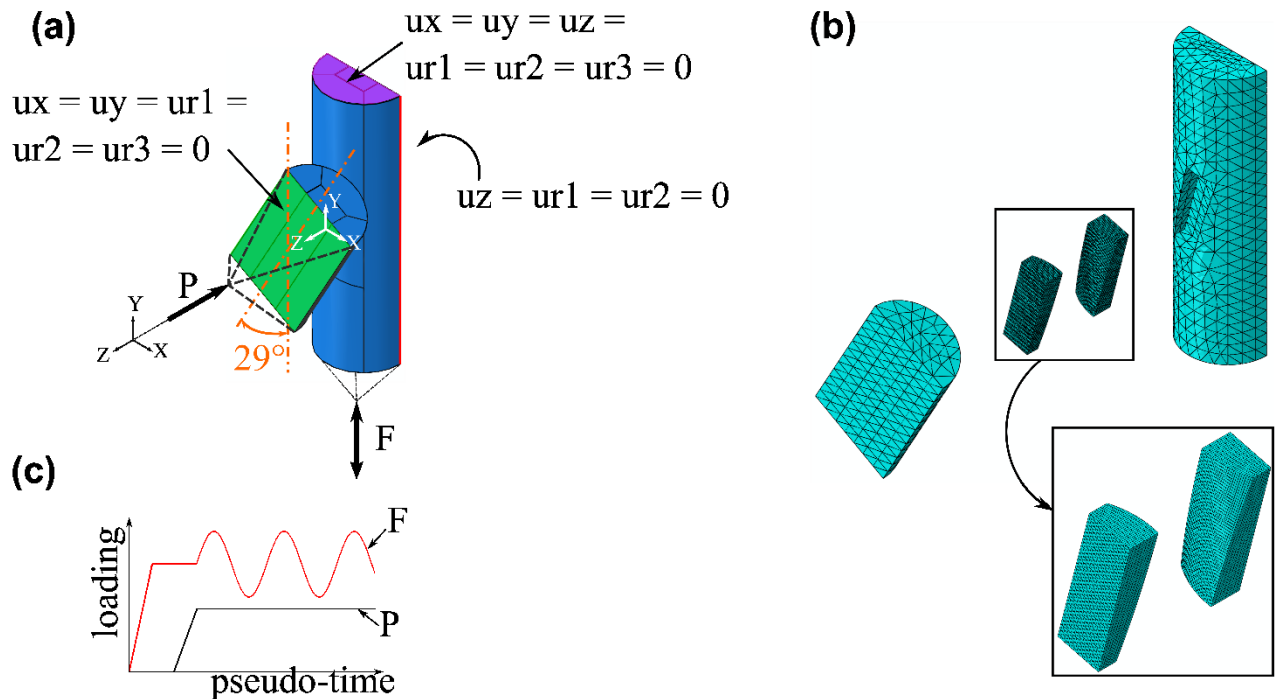


Fig. 2.7. FE model of the contacting wires: (a) boundary conditions; (b) mesh; (c) loading history.

The mesh of the two contacting wires is shown in Fig. 2.7b. Far from the contact surface, a coarse non-structured mesh of ten-node quadratic tetrahedral elements (C3D10 element) was created. Beneath the contact surface, a very fine mesh was required to compute the high stress gradients accurately. To accomplish this, a partition of eight-node linear brick elements with reduced integration (C3D8R element) was created beneath the contact surface. The partition consisted of 11200 brick elements in a volume of $500 \times 970 \times 2900 \mu\text{m}^3$, the characteristic dimensions of a single element being $30 \times 20 \times 50 \mu\text{m}$. In addition, 2422 and 5639 tetrahedral elements were used to mesh the bulk of the inclined and vertical wires, respectively. The Hertz solution for two elastic wires crossed at an angle of 29° and subjected to a normal load, as described by Johnson (1985), was chosen to check the accuracy of the finite element results. The difference between the simulated and analytical values for the pressure distribution and semi-axes of the elliptical contact area were found to be less than 10%.

The contact interaction between the wires was defined by the finite sliding formulation and the surface-to-surface discretization method available in Abaqus. The surfaces of the vertical and inclined wires were selected as master and slave, respectively. The Lagrange multiplier friction formulation was used to describe the tangential behavior. A friction coefficient of 0.6 was adopted in this work based on values reported in literature (Papailiou, 1997; Cloutier et al., 2006)

The loading history was applied in three steps, as shown in Fig. 2.7c. First, a remote mean load is applied to the bottom surface of the vertical wire, then a fixed normal load P is applied to the symmetric surface of the wire and, finally, the remote mean load is superposed to a cyclic load with a constant amplitude.

2.5 Results and discussion

The material constants of the fatigue life prediction methodology under evaluation in this work are based on test data from plain and sharply notched specimens. First, the constants of the SWT vs. fatigue life relationship, Eq. (2.3), were determined by best fitting the test data from plain wires

subjected to fully reversed loading (Table 2.1). For the data under consideration, $\alpha = 221 \text{ MPa}$ and $\beta = -0.0679$.

The determination of the characteristic length vs. fatigue life (L vs. N_f) relationship was made from a data set of notched specimens. This was achieved by developing a python script that process the stress distribution in the vicinity of a notch, which was obtained by the finite element models described in Section 2.4. For each test data, the python script finds the characteristic length of the damage zone for which the fatigue life predicted by the SWT parameter equals the observed life. The $L-N_f$ diagrams obtained from the test data of circumferentially V-notched wires (Table 2.2) and of the wires with transverse circular hole (Table 2.3) are shown in Fig. 2.8. A glance at these figures reveal that the $L-N_f$ data can be described by a power law relationship. Best fitting of the test data of the circumferentially V-notched wires yielded $\gamma = 17036 \text{ }\mu\text{m}$ and $\delta = -0.3224$, while for the wires with transverse circular hole $\gamma = 9522 \text{ }\mu\text{m}$ and $\delta = -0.2814$. Most of the calibration data were found within a factor of 3. Fig. 2.8 also shows an overlapping of calibration data of the two notches for the studied range of life, this result indicates that the AA1350-H19 is not strongly affected by the type of notch used on calibration method.

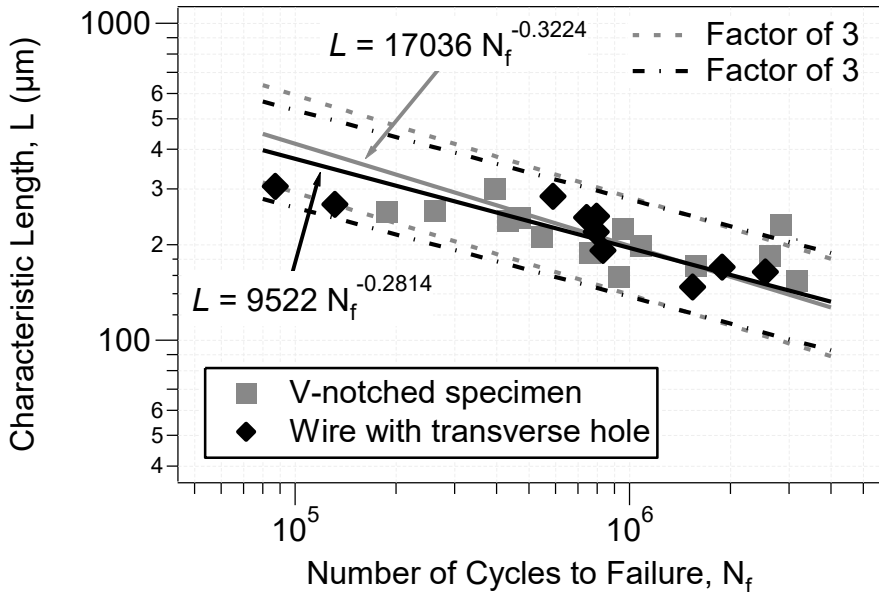


Fig. 2.8. Correlation between the characteristic length and the number of cycles to failure obtained using test data from V-notched wires and wires with transverse hole.

Regarding the fatigue life predictions of the two contacting wires, the damage zone regions was centered on the upper and lower edges of the contact between wires, so as on the center of the contact between wires. It was observed that all critical life estimates were found on the lower edge of the contact.

Life predictions of the wire-wire fatigue tests are compared with the observed lives in Fig. 2.9. The open and solid symbols denote the life predictions made using the constants obtained from the circumferentially V-notched wires and from the wires with transverse circular hole, respectively. The solid diagonal line represents a perfect agreement between the estimated and observed number of cycles to failure, and the dashed lines are the factor-of-three boundaries. Most of the predicted lives were conservative and were within the factor-of-three boundaries. Such a range is similar to the scatter of the test data used to calibrate the fatigue life prediction model. The estimated number of cycles to failure were not significantly altered by the data set used to calibrate the fatigue life prediction methodology.

The fatigue life model investigated in this work provides a good trade-off between accuracy and complexity. One appealing feature of the model is that the material constants can be determined from simple fatigue tests on plain and notched wires. Furthermore, the model makes use of stresses obtained by assuming a linear, elastic material behavior, thus simplifying the finite element simulation of two contacting wires under cyclic loading. It is possible to perform a detailed stress-strain analysis of the wire-wire contact problem, but the cyclic plasticity material behavior and possibly the wear process must be included in the analysis. Taking these details into account would result in a very complicated model, and additional experiments would be required to determine the material constants. Also, the computation time of the finite element-based contact problem will slow down.

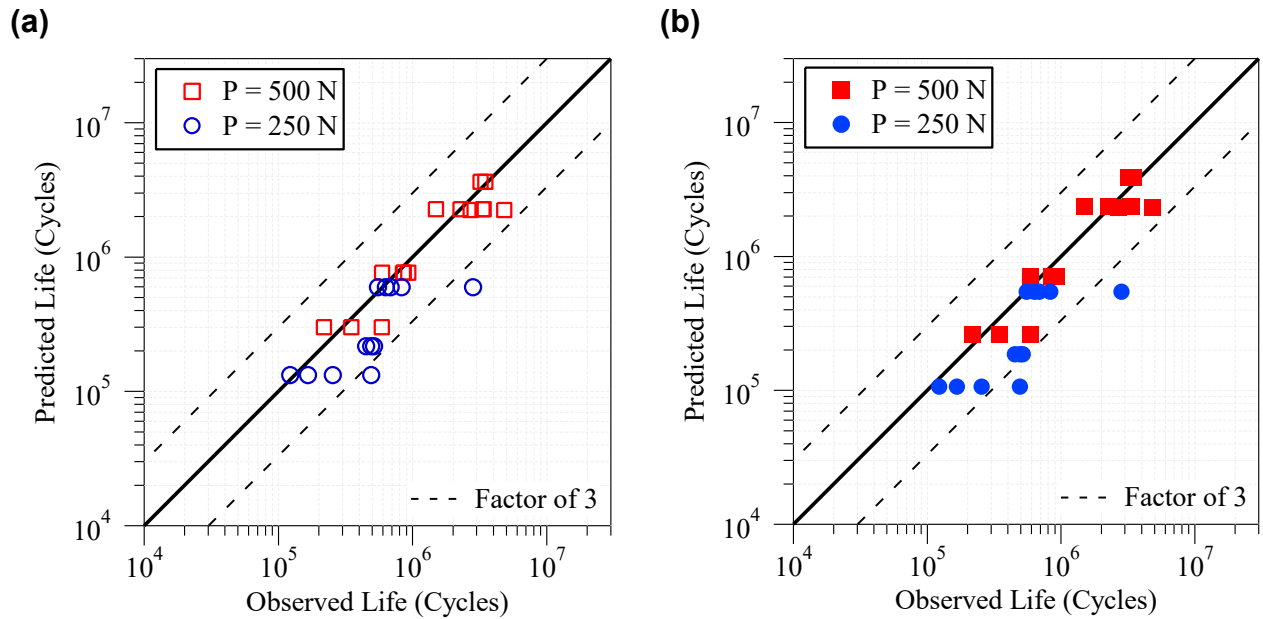


Fig. 2.9. Observed life versus predicted life for the wire-wire tests. Fatigue model calibrated using test data from (a) V-notched wires and (b) wires with transverse hole.

2.6 Conclusions

Wires made of 1350-H19 aluminum alloy taken from ACSR (Aluminum Conductor Steel Reinforced) overhead conductors were investigated in this work. Fatigue experiments were conducted on circumferentially V-notched wires, wires with a transverse hole, and two contacting wires with a crossing angle of 29° . Based on the experimental results and analysis presented in this work, the following conclusions can be drawn:

- (1) Circumferentially V-notched wires with an opening angle of 60° and notch root radius of 0.17 mm, and wires with a transverse hole with a diameter of 0.7 mm, yielded test data within a factor-of-three scatter band in the observed lives. It was shown that a non-local version of the Smith-Watson-Topper fatigue model can be successfully calibrated using such test data.
- (2) Most of the fatigue life estimates of the wire-wire tests were within factor-of-three boundaries, which is a range similar to the scatter of the calibration data.
- (3) Fatigue life estimates of the wire-wire tests were essentially the same when the test data from circumferentially V-notched wires or wires with a transverse hole were used to calibrate the fatigue model.

(4) The non-local version of the Smith-Watson-Topper fatigue model used in this work provided a good trade-off between accuracy and complexity. One simplifying assumption is the use of stresses obtained from a linear, elastic analysis. Furthermore, material removal due to wear is not considered. Despite of these simplifications, fatigue life estimates of the wire-wire tests were achieved with reasonable accuracy.

3 Experimental–numerical methodology for the determination of the loading conditions of two contacting wires of the AAAC 900 MCM conductor

3.1 Introduction

The structural integrity of overhead conductors is vital for the safe and stable operation of transmission lines and has been of great concern in the design and maintenance stages. A potential failure mode in overhead conductors is the rupture of wires caused by fretting fatigue damage, especially at regions where the movement of the conductor is restrained, such as at suspension clamps (Cardou et al., 1992; Zhou et al., 1994b).

Full-scale tests have been carried out over years to understand the global mechanical behavior of overhead conductors. Several studies regarding the fatigue behavior of conductors have revealed that their life performance is strongly influenced by bending stress amplitude, mean tensile load, suspension clamp geometry, clamping force, and type of conductor (Cardou et al., 1990; Cloutier et al., 2006; Azevedo et al., 2009; Lévesque et al., 2010; Fadel et al., 2012; Baumann and Novak, 2017).

Although full-scale testing of overhead conductors is of great importance, such tests are expensive and technologically difficult to perform. Furthermore, fatigue failures of overhead conductors actually occur at the local (wire) scale, more specifically at the contact region between wires or between outer-layer wires and clamp. Therefore, experiments and analyses of local contact systems (wire-wire or wire-clamp) may lead to a better understanding of the fatigue performance of overhead conductors.

Limited work has been done on the mechanical interaction between two wires of an overhead conductor, or between a wire and the clamp. Zhou et al. (1996) conducted fretting fatigue tests on a single wire in contact with the surface of a suspension clamp and concluded that typical features of the damage process (e.g., fretting patterns, crack propagation modes, and number of cycles to crack initiation) were similar to those observed on full-scale tests. Lévesque et al. (2011a) performed an

elastic-plastic finite element simulation of the contact problem between a wire and the bed of a suspension clamp, and a fatigue analysis based on a damage parameter proposed by Ruiz et al. (1984) was performed. Further finite element results obtained by Lévesque et al. (2011b) showed that an elastic-plastic contact model between two wires could provide contact area and contact force in good agreement with experimental results for different crossing angles. The effect of the mean tension on the contact between two wires was also studied by Lévesque and Légeron (2011) by conducting finite element simulations. It was concluded that static tension had little influence on the contact stresses of the two-wire contact problem investigated.

A thorough search of the relevant literature revealed limited scientific contributions on determination of local loading conditions of wires of overhead conductors. The present study has the objective to provide a methodology to determine local forces on aluminum wires based on critical region conditions of overhead conductors using numerical and experimental approaches. Previously tested conductors (Badibanga, 2017) were examined to carry out this analysis.

3.2 Observation of the fatigue-critical region of the AAAC 900 MCM conductor

The overhead conductor investigated in the present work is designated as AAAC 900 MCM. This conductor contains a total of 37 wires of 6201-T81 aluminum alloy, each having a diameter of 3.96 mm. The wires are distributed in three layers plus the central wire. The nominal diameter of the conductor is 27.74 mm.

The first step of the experimental program consisted in identifying the fatigue-critical region of the conductor, i.e. the region where wire breakages most frequently occurred, and to map the spatial distribution of the observed failures. To this end, fatigue tests on the AAAC 900 MCM conductor were carried out in the Laboratory of Fatigue and Structural Integrity of Overhead Conductors of the University of Brasilia. The laboratory is equipped with three resonance fatigue test benches, as shown schematically in Fig. 3.1. Each bench has a total length of 47 m, being 40 m of active span and 7 m of passive span. One end of the conductor is anchored in a fixed block (block

1). The conductor is assembled in a suspension clamp which is rigidly attached to a metallic cradle mounted on a movable concrete block (adjustable block). The suspension clamp is placed inclined in 10° with respect to horizontal, such angle is a typical value for laboratory tests (CIGRÉ, 2007) in order to reproduce the static bending due to sag of the conductor. The other end of the conductor is fixed to a lever arm (block 3) which is loaded by a dead weight. The static tension load is applied to the conductor by the lever arm and the hand traction winch positioned on the opposite side of the bench.

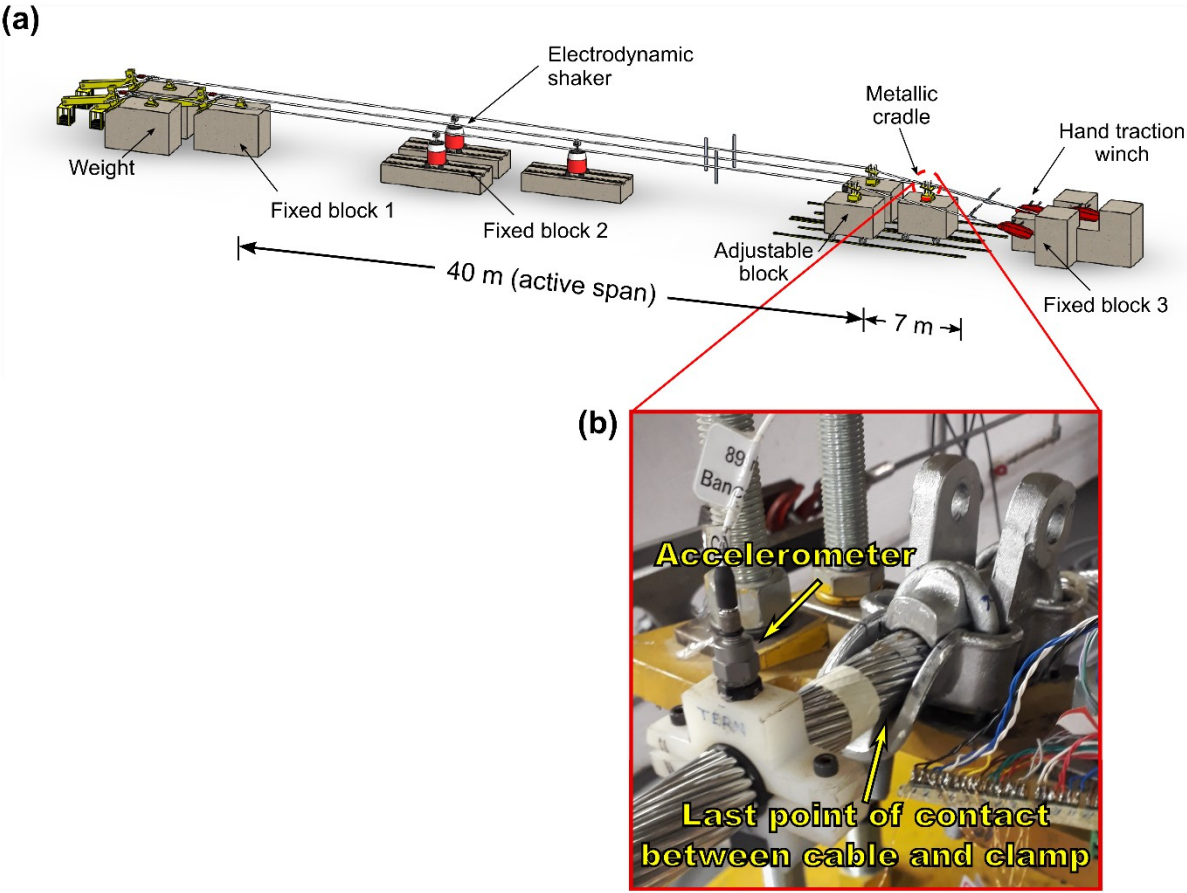


Fig. 3.1. (a) Schematic of the resonance fatigue test benches of the Laboratory of Fatigue and Structural Integrity of Overhead Conductors of the University of Brasilia, and (b) Conductor assembled with suspension clamp.

The excitation of the conductor is produced by an electrodynamic shaker, which is located on the fixed block 2 and is connected to the conductor within the active span. The test is controlled by a prescribed displacement measured by an accelerometer positioned at 89 mm from the last point of

contact between cable and suspension clamp. The output signal of the accelerometer is part of a closed loop control system that assures that the shaker works to maintain the same peak-to-peak displacement at 89 mm from the conductor-clamp last point of contact. To define the test frequency, a resonance sweep is carried out and the closest value to one of the resonance frequencies is chosen to run the test. More details on the conductor fatigue test bench can be found in references (Azevedo et al., 2009; Fadel et al., 2012; Steier et al., 2014).

The fatigue tests performed on the AAAC 900 MCM conductor are shown in Fig. 3.2 in a stress amplitude vs. number of cycles to failure diagram. As often done in fatigue studies of overhead conductors, the stress amplitude was defined as the bending stress amplitude obtained from the following formula developed by Poffenberger and Swart (1965):

$$\sigma_a = \frac{E_a d T / EI}{4 \left(e^{-\sqrt{T/EI} x} - 1 + \sqrt{T/EI} x \right)} Y_b \quad (3.1)$$

where σ_a is the bending stress amplitude at the last point of contact of the conductor-clamp assembly, and Y_b is the peak-to-peak displacement at 89 mm from the conductor-clamp last point of contact. E_a and d are the Young's modulus and the diameter of an aluminum wire of the outermost layer of the conductor, respectively. T is the static tension experienced by the conductor, and EI is the minimum flexural stiffness of the conductor. x is the distance between the last point of contact of the conductor/clamp assembly and the point where the vertical displacement is measured. For the AAAC 900 MCM conductor under investigation, $E_a = 69$ GPa, $d = 3.96$ mm, $EI = 3.09 \times 10^7$ Nmm², and $x = 89$ mm. The remaining parameters were specified as follows.

All tests were performed under a static tension load of 26.3 kN, which was 20% of the rated tensile strength of the conductor. Three levels of peak-to-peak displacement at 89 mm from the conductor-clamp last point of contact were considered in the tests: 0.68 mm, 0.81 mm and 0.9 mm. According to Eq. (1), these displacements correspond to bending stress amplitudes of 23.7 MPa, 28.2 MPa and 31.4 MPa. The fatigue tests were replicated three times for each stress amplitude.

Failure criteria was defined as rupture of 4 conductor’s wires. Each test was stopped after four wire breaks and the recorded number of loading cycles was defined as the number of cycles to failure.

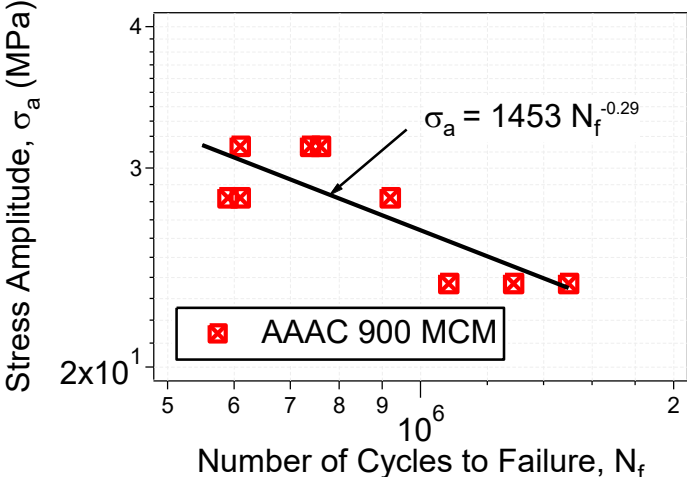


Fig. 3.2. S-N curve for AAAC 900 MCM conductor static tensile load of 26.3 kN.

After the tests, each conductor was unwrapped and the locations where wires breaks occurred were identified. This procedure was performed with the aim of determining the critical region of the conductor, i.e. the region where most of the wire breaks took place. The mapping of the wire breaks was first carried out according to their position within the cross section of the conductor. Then, the distance from the keeper edge where the wire breaks occurred were recorded.

The location of wire breaks within the cross section of the conductor followed the terminology shown in Fig. 3.3. Wire breaks found at the upper part of the cross section and at the external (outermost) layer were designated as Upper & External, and those found at the upper part of the cross section and at any internal layer were designated as Upper & Internal. In the same way, Lower & External refers to failures observed at the lower part of the cross section and at the external layer, and Lower & Internal to failures that occurred at the lower part of the cross section and at any internal layer.



Fig. 3.3. Terminology for the identification of the location of wire breaks within the cross section of the AAAC 900 MCM conductor.

Breakages were observed in three combinations of the categories aforementioned, Fig. 3.4 shows the percentage of failures distributions of each stress amplitude for the following combinations: Upper & External for failures found at upper section and external layer of the conductor; Upper & Internal for failures at upper section and any internal layer; and Lower & External for failures at lower section and outermost layer of the conductor. No failure was observed on lower part and inner layer of the conductor.

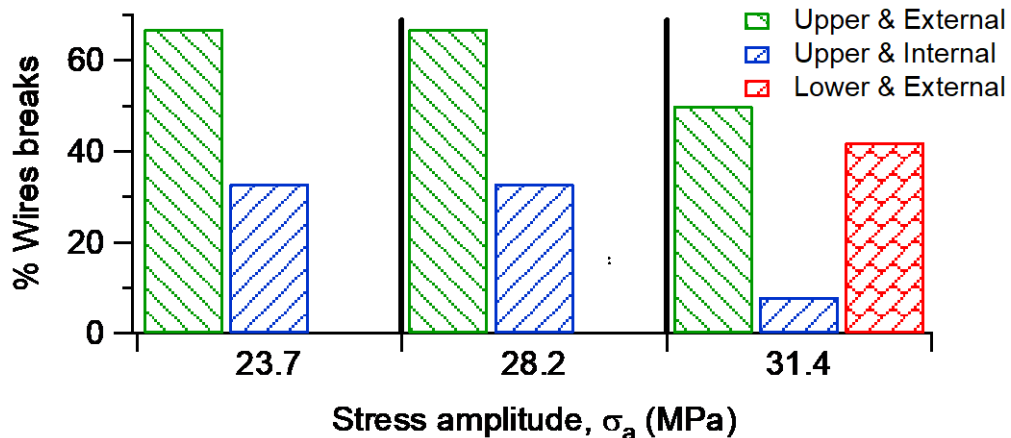


Fig. 3.4. Distribution of wire breaks within the cross section of the conductor for different stress amplitudes.

Figure 3.4 shows the distribution of wire breaks within the cross section of the conductor for each of the stress amplitudes investigated. For example, for a stress amplitude of 23.7 MPa all wire breaks were observed at the upper part of the cross section, being 67% at outermost layer and 33% at the inner layers. A glance at Fig. 3.4 reveals that among all the observed wire breaks, most of them took place at the external layer of the upper part of the conductor. Also, all wire breaks found

for bending amplitudes of 23.7 MPa and 28.2 MPa occurred at the upper part of the conductor. Despite the majority of failure occurrences found on the upper part of the conductor, the test under stress amplitude of 31.4 MPa also presented a considerable number of failures (42%) at the lower part of the conductor. This indicates that higher stress amplitudes may change the critical region of the AAAC 900 MCM conductor. It is also important to note that no wire break was observed at the inner layers of the lower part of the conductor.

The next step of the procedure for mapping the spatial distribution of the wire breaks consisted in measuring the distance from the keeper edge at which the wire breaks occurred. Due to their preponderant number of occurrences, only the wire breaks observed on the upper part of the external layer of the conductor were considered in the analysis.

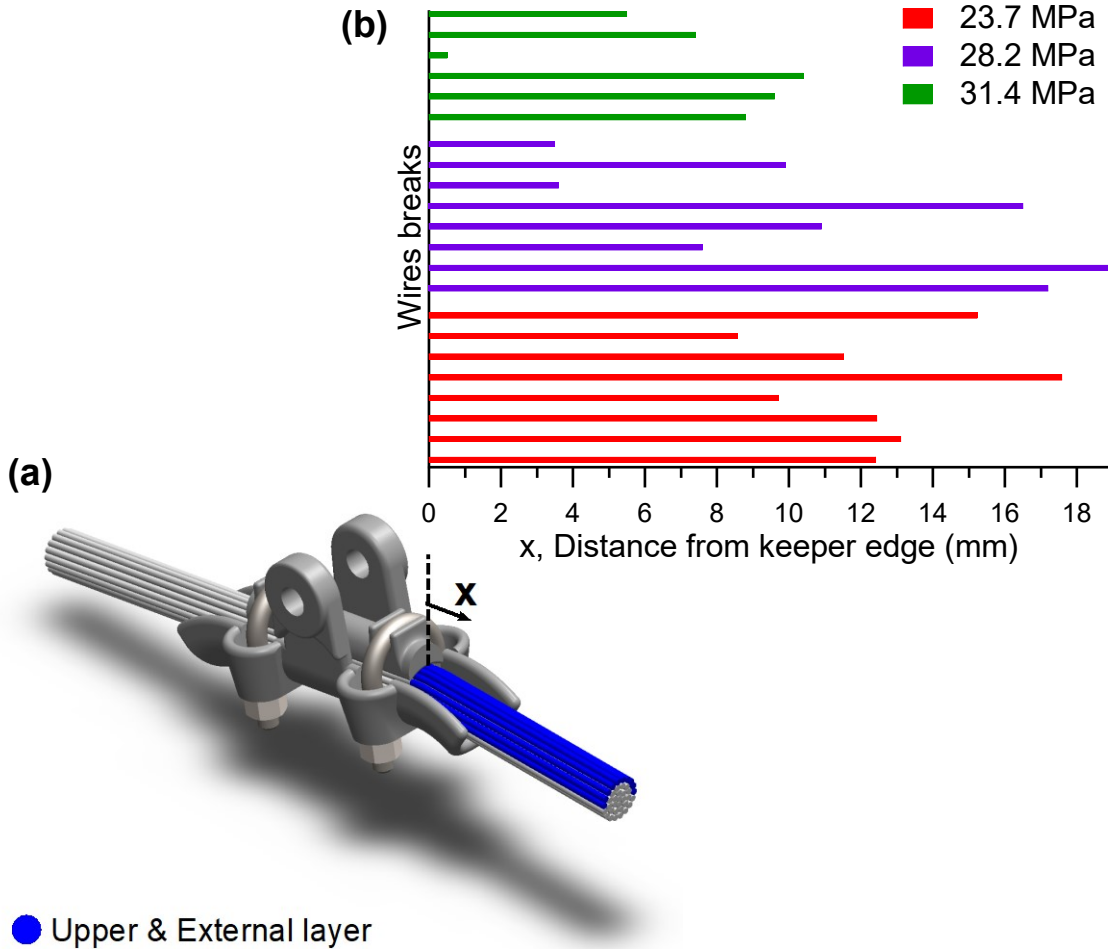


Fig. 3.5. (a) Coordinate distance from keeper edge of the conductor/clamp assembly; (b) Distances of wire breaks observed at the external layer of the upper part of the conductor.

Figure 3.5a shows the coordinate axis used to measure the distance of the wire break from the keeper edge and also indicates the wires that were analyzed, and each bar on Fig. 3.5b represents the observed distances for each of the stress amplitudes studied. It is seen that the locations where the wire breaks were found depended on the magnitude of the bending stress amplitude. For $\sigma_a = 31.4$ MPa, breakages ranges between 0.5 and 10 mm; $\sigma_a = 28.2$ MPa failures were observed from 3 mm up to 19 mm; and $\sigma_a = 23.7$ MPa the observed failure region varies between 8.5 mm and 17.5 mm. Interestingly, the positive values shows that all failures occurred ahead of the keeper edge in a range between 0.5 and 19.0 mm. Such information indicates that cracks initiations took place at the contact interface between wires of outermost layer and wires just beneath them.

3.3 Estimation of the loading conditions of two contacting wires of the fatigue-critical region of the conductor

The post-failure observations described in Section 3.2 indicated that the external layer of the upper part of the AAAC 900 MCM conductor is a fatigue-critical region. In this section, an experimental-numerical procedure for estimating the loading conditions of two contacting wires located at such a critical region of the conductor is presented.

The reasons for estimating the loading conditions of two contacting wires of an overhead conductor were:

- (1) it may help verifying and improving finite element models of conductor-clamp assemblies (Qi, 2013; Lalonde et al., 2018), and
- (2) fatigue testing on two contacting wires is important for understanding the damage process at the local (wire) scale (Zhou et al., 1996; Lévesque et al., 2011a; Lévesque and Légeron, 2011). To perform such kind of tests within a reasonably realistic scenario, a knowledge of the magnitude of the loads acting on two contacting wires is required.

The estimation of loading conditions of wires located at regions where the conductor movement is restricted can be challenging due to combined tensile and bending loading applied to the

conductor. Due to wrapping angle of the cable, the tensile load applied to the cable cause on adjacent wires radial contacting load. Therefore, during the bending process of the cable, the interactions between contacting wires produce friction loads that may prevent relative slip between adjacent wires. Whenever loads that cause sliding are greater than friction, a wire may experience a relative displacement with respect to neighbors ones. Such wire-wire interactions provide to the cable the desirable flexibility but also is responsible for the complexities involved in the process of estimating the loading conditions of wires of such component during service loading applications.

An experimental methodology used by Ouaki et al. 2002 and Lévesque et al. 2010 is capable to distinguish bending strains and traction strain within a wire of an overhead conductor by removing wires located on the sides of a studied wire and fixing two gages and one central strain gages on the wire of interest. It can be observed from both studies that during static tests bending considerably affects the strain state of the analyzed wires, but during dynamic tests, static strain amplitude is much higher than bending amplitude strains.

Regarding the fatigue tests carried out on the AAAC 900 MCM, the failure analysis presented on section 3.2 revealed that wire ruptures occurred up to 20 mm ahead of the keeper edge (Fig. 3.5). Inspections on the clamp used during the fatigue tests on the AAAC 900 conductor indicates that part of the critical region of failure – from keeper edge up to last point of contact between cable and clamp – is located in a region where the longitudinal clamp profile is flat. No static bending of the cable occur at such region, thus bending of wires is not expected. Static bending is expected on the remaining section of the critical region since it lays in a zone of the clamp where its longitudinal profile is curved. For the sake of simplicity, loading estimates on wires from the critical region are considered as traction only.

In what follows, the estimation of the loading conditions of two contacting wires of the AAAC 900 MCM conductor is demonstrated for the tests performed at a bending stress amplitude, σ_a , of 23.7 MPa. The loading conditions that will be estimated are:

- the mean tensile stress due to the static tension force experienced by the cable;
- the bending stress amplitude caused by the cyclic displacement prescribed at 89 mm from the conductor-clamp last point of contact;
- the interwire normal contact force due to the stretching and clamping of the conductor.

3.3.1 Estimation of the mean bulk force

Several studies about strain distribution of cables in cable/clamp assemblies shows that static strains are considerably higher at the region near the suspension clamp (Cardou et al 1993, Lévesque et al. 2010). Strain measurements done by Ouaki et al. 2002 revealed that wires at regions near the suspension clamp are subjected to strain levels up to 3.5 times higher than strains on a free span region of the cable.

To measure such strains and to estimate the mean bulk force of wires at the critical region of the conductor, a static test was carried out. The cable was subjected to a mean tensile force of 26.3 kN and axial strains were obtained from strain gages located at wires on the critical region of the cable.

As shown in Fig. 3.6, nine strain gages were glued on the three top wires in the region close to the keeper. Three strain gages were glued just beneath the keeper edge. Other three strain gages were fixed on the region diametrically opposed to the last point contact of the conductor-clamp assembly, which is 9.8 mm ahead of the keeper edge. Another three strain gages were attached 20 mm ahead of the of the keeper edge. A single strain gauge was attached to a wire at 2 m distant from the conductor-clamp assembly to assess axial strain in a free span region of the cable.

To obtain the static strain measurements, the strain gages were balanced at a tensile load level equal to 1% of the rated tensile strength of the conductor. Then, the cable was tensioned up to 26.3 kN tensile load and torque was applied to suspension clamp nuts. Strain gages 5 and 9 stopped to work before the measure could be done.

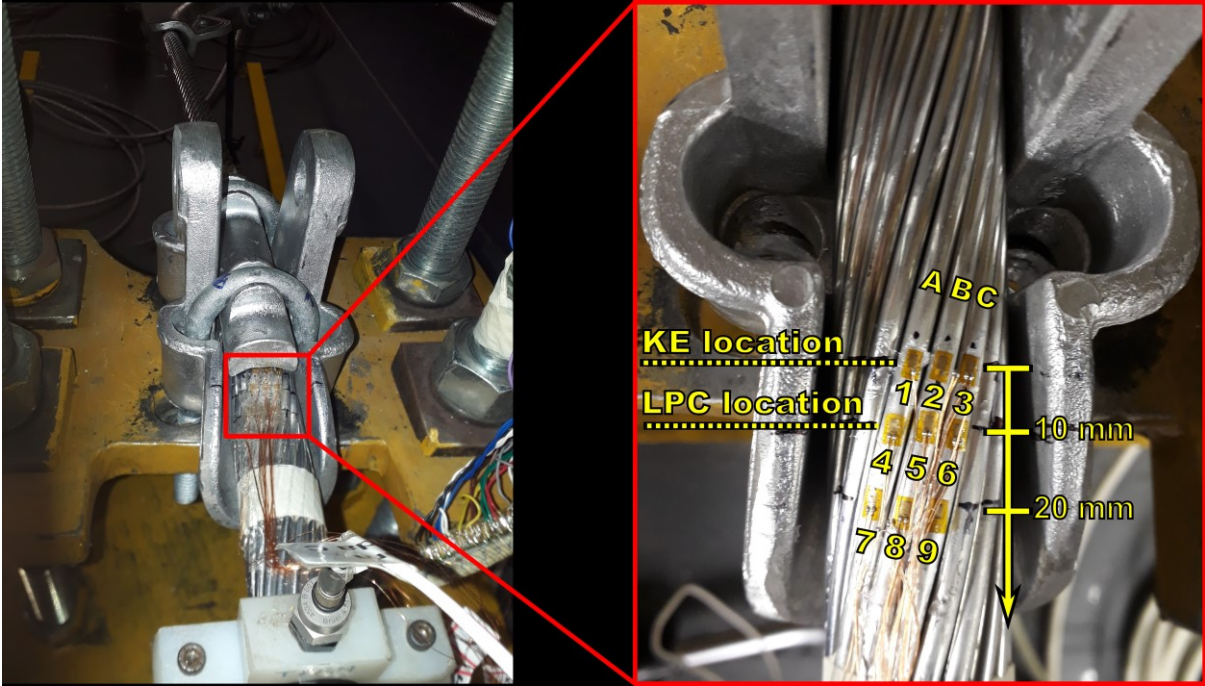


Fig. 3.6. Strain gages located at the fatigue-critical region, in detail: keeper edge (KE) location, region diametrically opposed to the last point of contact (LPC) between conductor and clamp, and location 20 mm ahead of KE.

Figure 3.7 illustrates strain measurements obtained from the static test. The strain levels were obtained for the moments before and after the application of clamping force. It can be observed that the clamping has strong effects on strains at the region close to the keeper edge. At such region, strains can reach up to 3520 $\mu\text{m}/\text{m}$. Fig. 3.7 also shows the fast decay on strain level in the 20 mm length analyzed, it is attributed to the local effect of clamping in addition to the cable changing of direction due to clamp inclination (10°). The strain measured at 2 m from the clamp was equal to 770 $\mu\text{m}/\text{m}$, when compared to strains measured near the clamping region, it ranges between 4.57 to 1.46 times lower.

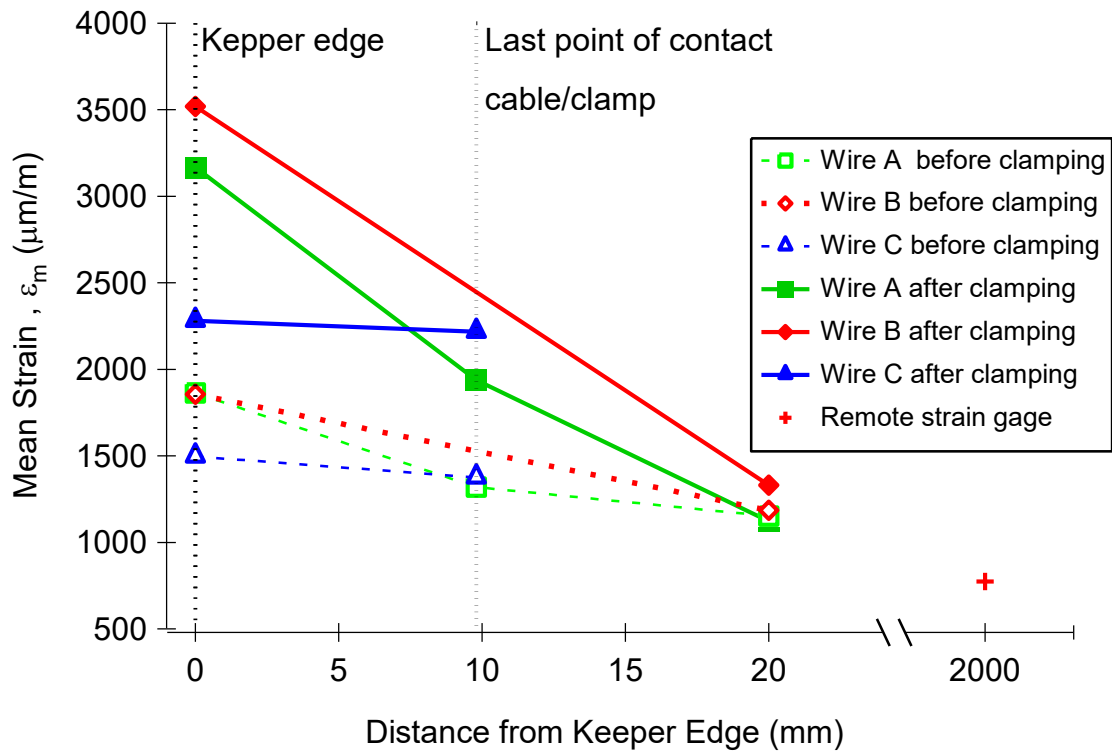


Fig. 3.7. Static strain distribution on wires A, B and C for a mean tensile load equal to 26.3 kN.

It can be observed that none of the strain measures exceeded the yield strain (6435 $\mu\text{m}/\text{m}$), therefore to estimate the tensile stress it was assumed a linear elastic material behavior and uniform stress distribution over the wire cross section. Table 3.1 presents mean tensile stresses based on observed strain levels after the clamping of the cable.

Table 3.1. Strains obtained from strain gages attached at the critical region of the AAAC 900 MCM conductor, and estimated values of the mean stress experienced by the wires.

Strain Gage	$\epsilon_m(\mu\text{m}/\text{m})$	$\sigma_m = E \epsilon_m(\text{MPa})$
1	3168	218.6
2	3520	242.9
3	2281	157.3
4	1939	133.8
6	2217	153.0
7	1122	77.4
8	1330	91.8
10	773	53.4

3.3.2 Estimation of the bulk force amplitude

To estimate the bending stress amplitude of wires located at the critical region of the AAAC 900 MCM conductor, a cyclic test was carried out. In this test, the conductor was subjected to the same static tensile force, 26.3 kN, and a peak-to-peak displacement of 0.68 mm at 89 mm of the conductor-clamp last point of contact ($\sigma_a = 23.7$ MPa). The test was carried out up to 5×10^5 cycles, which is approximately half of the observed fatigue life of the conductor for this load condition (refer to Fig. 3.2). No wire break was detected during the test.

It must be observed that the cyclic test was carried out using the same configuration test from Section 3.1, however considerable discrepancy between strain measures and expected values from Poffenberger–Swart model was found. It is believed that such difference occurred due to slight changing of cable position in relation to the clamp during the unloading and re-loading of the cable. Therefore, results presented in the following are related to an additional cyclic test that was carried out using new strain gages fixed after the loading of the cable.

The bending stress amplitudes of wires located at the critical region of the conductor were determined from strain measurements. As shown in Fig. 3.8, three strain gages were attached very close to the keeper edge so as to assess the effect of clamping on the stress amplitude. Other three strain gages were glued on the region diametrically opposed to the last point contact of the conductor-clamp assembly, which is 10 mm ahead of the keeper edge.

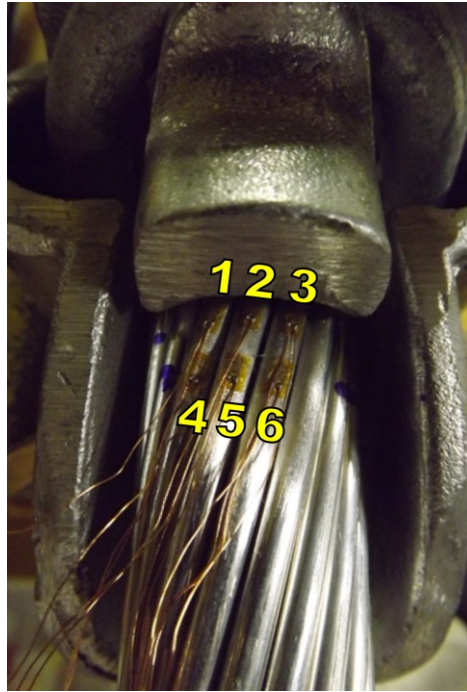


Fig. 3.8. Strain gauges fixed close to the keeper edge (1, 2 and 3) and on the region diametrically opposed to the LPC of the cable/clamp (4, 5 and 6).

The strain amplitudes obtained from each strain gage are presented in Table 3.2. To estimate the stress amplitude on a wire, it was assumed a linear elastic material behavior and a uniform stress distribution over the wire cross section. The Young's modulus of the 6201-T81 aluminum alloy is 69 GPa and the diameter of a wire is 3.96 mm. The resulting stress amplitudes and force amplitudes are also given in Table 3.1. It is noteworthy that the stress amplitudes estimated at positions 4, 5 and 6 (Fig. 3.8) were equal to the values given by the Poffenberger–Swart formula. These results have shown that the Poffenberger–Swart formula is suitable for the AAAC 900 MCM conductor under the investigated loading conditions. Note also that the strain amplitudes from strain gages located at the same distance from the keeper edge are practically identical. Slight differences of about 10% between the strain measurements at the keeper edge and at 11 mm ahead of it were also observed, which may indicate that the clamping force has some effect at the region just ahead of the keeper.

Table 3.2. Strain amplitudes obtained from strain gages attached at the critical region of the AAAC 900 MCM conductor, and estimated values of the stress experienced by the wires.

Strain Gage	ε_a ($\mu m/m$)	$\sigma_a = E\varepsilon_a$ (MPa)
1	316	21.8
2	316	21.8
3	318	21.9
4	344	23.7
5	344	23.7
6	344	23.7

3.3.3 Estimation of the normal contact force

A numerical-experimental procedure was adopted to estimate the normal contact force between two contacting wires of the critical region of the conductor. The general idea was to find the magnitude of the normal contact force for which the simulated contact mark and experimentally observed fretting marks were as close as possible. Details of the finite element model for the normal contact of two wires, the verification of this model, and the application of the model for estimating the normal contact load of wires of the AAAC 900 MCM conductor are presented in what follows.

3.3.3.1 Estimation of the normal contact force

The finite element (FE) software package Abaqus (2013) was used to simulate the normal contact of two wires of the AAAC 900 MCM conductor. The FE model of the contacting wires is composed of two wires inclined at an angle α with respect to each other (Fig. 3.9a). The model is assembled in such a way that the major semi-axis of the ellipse of contact is parallel to the z-axis. Only half of the wires were modeled to reduce the computation time.

Figure 3.9a shows that far from the contact surface, a coarse non-structured mesh of ten-node quadratic tetrahedral elements (C3D10 elements) was created. To accurately simulate the contact problem, a very fine mesh was generated at the region near the contact interface. To achieve this, partitions of eight-node linear brick elements with reduced integration (C3D8R elements) were created for both wires at this region (Fig. 3.9b). The tie constraint option available in Abaqus was applied to the interfaces of the surfaces composed of C3D8R and C3D10 elements to fuse the

displacement field at these regions. This technique allowed an easy control of the mesh size in the contact region and simplified the mesh design by eliminating the creation of an increasing level of refinement towards the region of interest. Each partition consisted of 74880 brick elements in a volume of $1000 \times 4500 \times 400 \mu\text{m}^3$, the characteristic dimensions of a single element being $30 \times 20 \times 50 \mu\text{m}$. In addition, 7245 tetrahedral elements were used to mesh the bulk of each wire.

The wire-wire contact pair interaction was defined by using the finite sliding formulation and the surface-to-surface discretization method available in Abaqus. The surfaces of the upper and lower wires were selected as master and slave, respectively. The penalty method (hard contact) was used to describe the normal behavior.

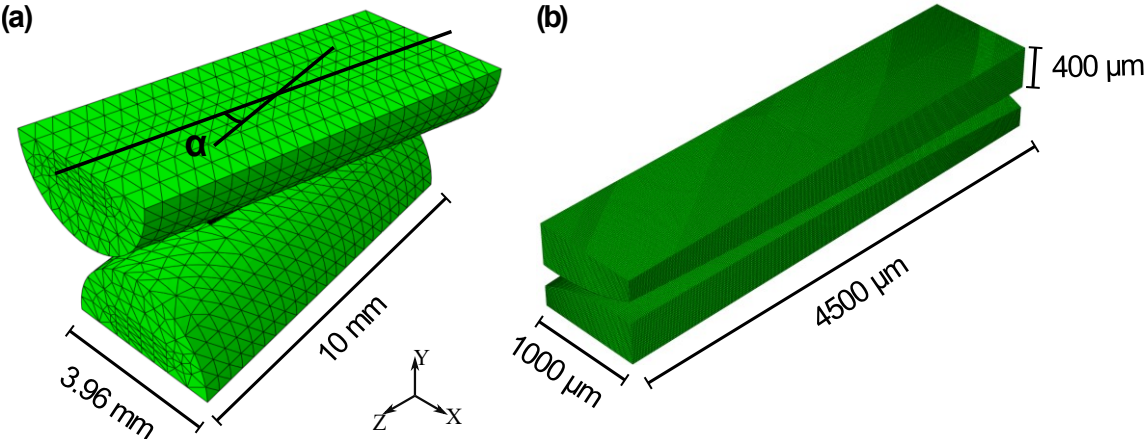


Fig. 3.9. FE mesh of the contacting wires: (a) global model; (b) fine mesh partitions on the contact region.

An elastic-perfectly plastic material model was used in the FE simulations. This material behavior was chosen based on the experimentally observed monotonic stress-strain curve of the 6201-T81 aluminum alloy, which is shown in Fig. 3.10. The monotonic tension test was performed on a wire extracted from the AAAC 900 MCM conductor using a displacement rate of 1 mm/min. The strain was measured during the test by a MTS 634.11F-24 extensometer. The monotonic properties of the material were as follows: Young's modulus of 69 GPa, 0.2%-offset yield stress of 306 MPa, and ultimate tensile strength of 311 MPa. The Poisson's ratio of the material was assumed

as 0.33. It is noted that the observed tensile strength of the material was consistent with the minimum break stress of 303 to 317 MPa reported by some overhead conductors manufacturers.

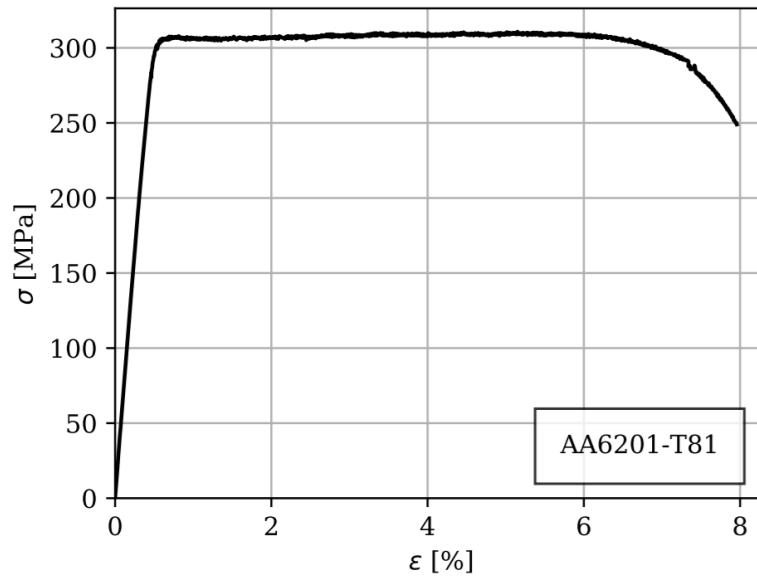


Fig. 3.10. Stress-strain curve of AA 6201-T81 wire extracted from AAAC 900 MCM conductor.

Simple boundary conditions were applied to the FE model. A surface-based coupling was used to apply boundary conditions to the wires, this constraint couples the displacement of all nodes on a defined surface to the displacement of a reference point. All node displacements of the bottom surface of the lower wire were restrained, while only vertical displacements were allowed to the upper wire.

The loading history consists on the application of a vertical load to the symmetric surface of the upper wire in order to produce the contact between wires. Negligible difference between contact mark size during load application and plastic mark after removal of such contact load have been found, so contact load removal was not done.

3.3.3.2 Procedure for the determination of the normal contact force

The determination of the normal contact force is done using a Python script that compares the size of an experimental mark with the size of the numerical contact mark for each load increment given by the FE simulation.

Figure 3.11 illustrates the procedure to obtain the contact force. Given the size of an experimental elliptical contact mark between two wires, the algorithm calculates the percentual difference between the size of semi-axes of experimental elliptical contact mark, a_{exp} and b_{exp} , and the semi-axes of the numerical mark, $a_{num, i}$ $b_{num, i}$, for each contact load increment, $P_{num, i}$ using Eq. 3.2. The predicted contact load, P_{pred} , given by Eq. 3.4 is determined as the one which generates the minimum percentual difference between numerical and experimental contact dimensions, Eq. 3.3.

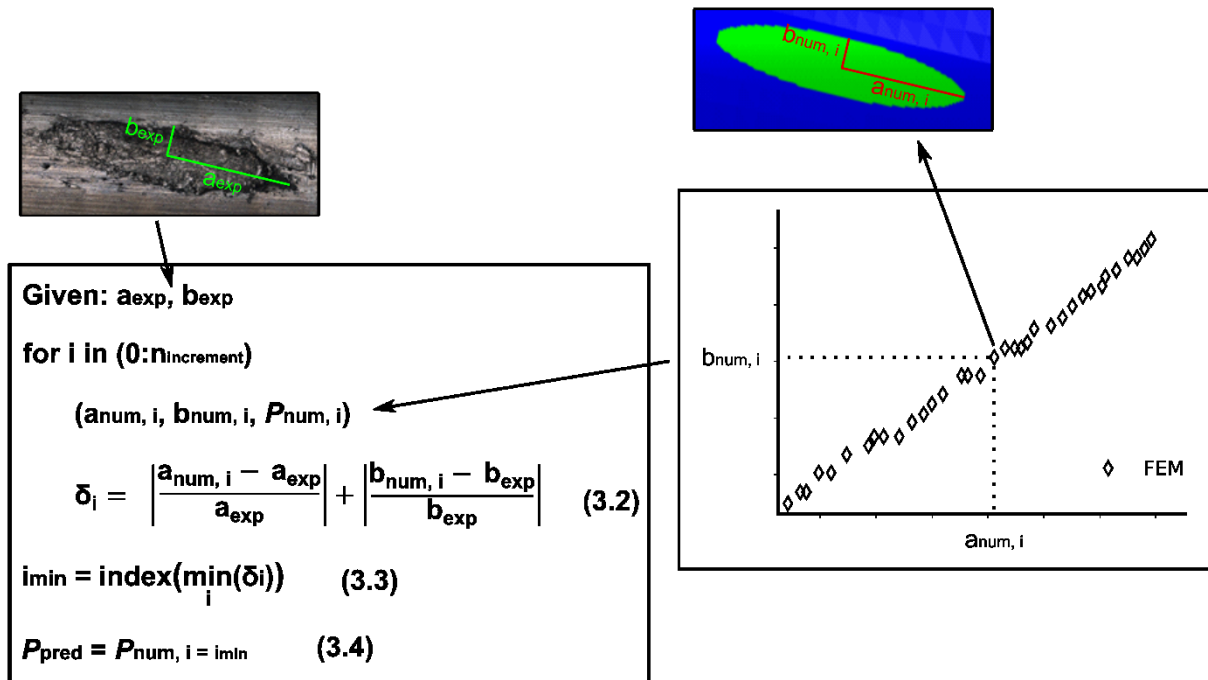


Fig. 3.11. Script used to determine the normal contact load between two wires.

Experimental contact marks between two crossed wires were generated for different levels of contact forces in order to assess the quality of the method presented on section 3.3 to predict the normal contact force. The contact marks were generated using the experimental apparatus shown in Fig. 3.12. A lower hydraulic actuator allows the application of remote loading to the specimen (vertical wire) and an upper hydraulic actuator controls the application of a tangential loading. Pneumatic actuators apply the normal contact load to the pad (oblique wire) and a bearing, and a digital control system ensures that the normal load is kept at a fixed level. The apparatus allows to adjust the crossing angle of the two wires so as to reproduce the angle between wires of adjacent layers of an overhead conductor.

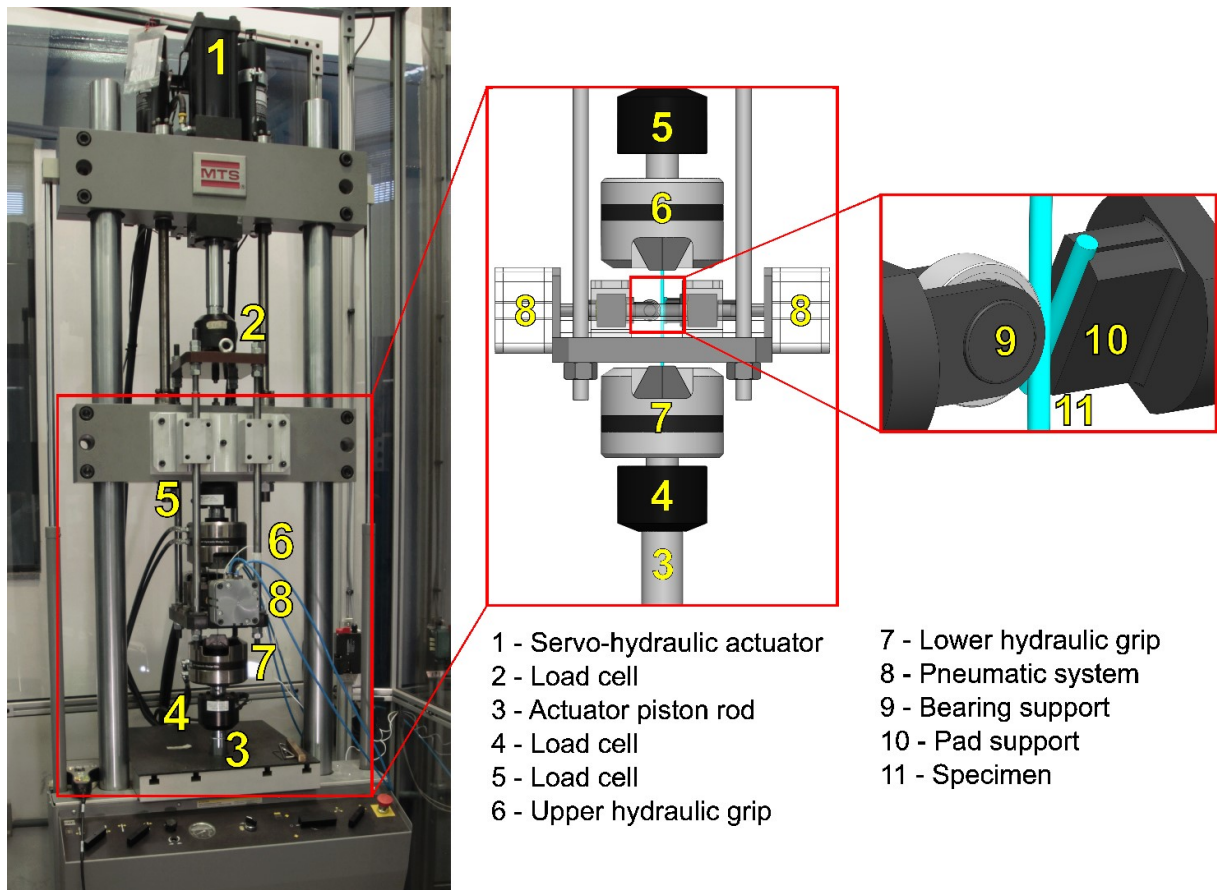


Fig. 3.12. Experimental apparatus for fatigue testing of two contacting wires.

The contact marks were generated using wires taken from the AAAC 900 conductor. The wires were crossed at an angle of 20° , four levels of contact loads were tested: 200, 300, 400, 500, 600, 700, and 800 N and no remote load was applied to the specimen. Lévesque and Légeron (2011) observed that remote load has negligible effect on contact conditions of two wires. After the tests, the elliptical contact marks had its major and minor semi-axes measured using a Confocal microscope. These values were used to determine the normal contact load between wires according to Eq. 3.3.

Based on contact marks generated using the experimental apparatus, Fig. 3.12, the contact load prediction methodology was assessed. The seven levels of contact load were tested, $P = 200, 300, 400, 500, 600, 700,$ and 800 N for wires crossed at an angle of 20° . Then the size of major (a) and minor (b) semi-axis of the elliptical contact areas were measured using a Confocal microscopy.

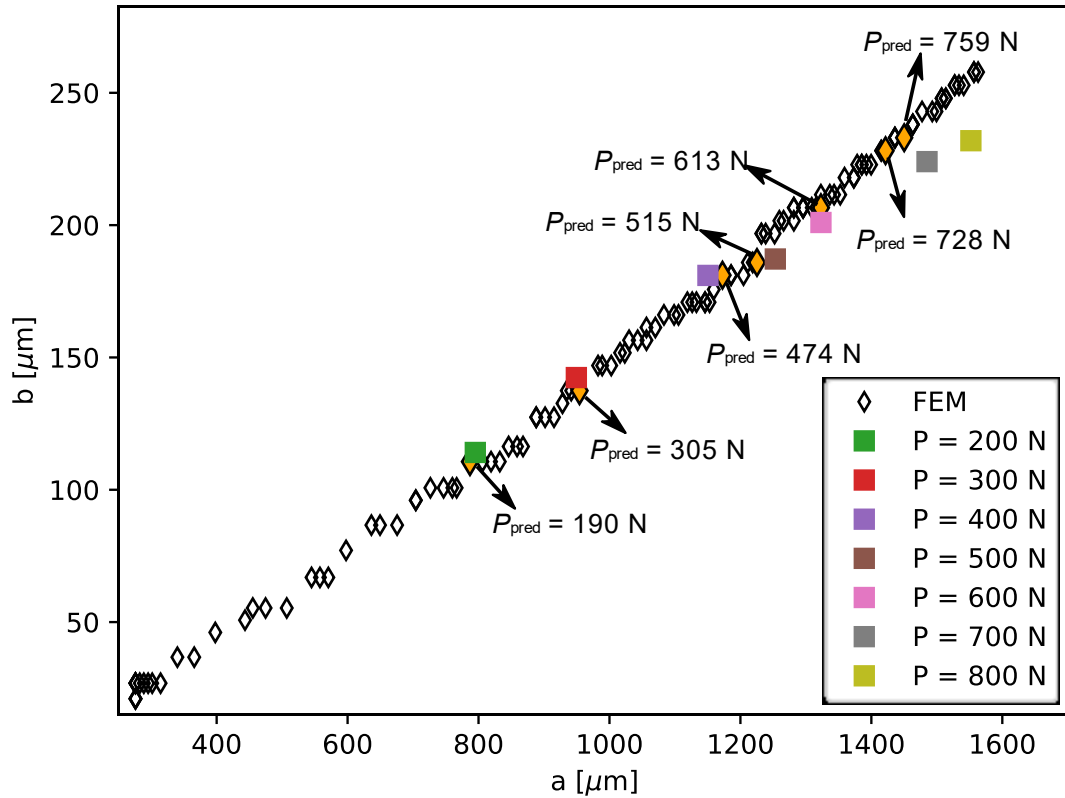


Fig. 3.13. Major vs. minor semi-axis measurements for different contact load levels.

The measured size of each mark was used to predict the contact force, Fig. 3.13 shows reasonable agreement between numerical and experimental values for semi-axis sizes for different contact loads. Orange diamond symbols represents the numerical values of semi-axis sizes that best matches with the experimental marks according to Eq. 3.3, P_{pred} is the predicted load to cause such marks.

3.3.3.3 Estimation of the normal contact force for wires of the AAAC 900 MCM conductor

After the half-life cyclic test, samples of the three upper wires were taken to microscopy analyses. As shown in Fig. 3.14, a region of 30 mm in length from keeper edge had all contact marks between adjacent layers measured using a Confocal microscope. Semi-axes of the elliptical fretting marks so as the angle between the major semi-axis and the wire principal axis were measured.

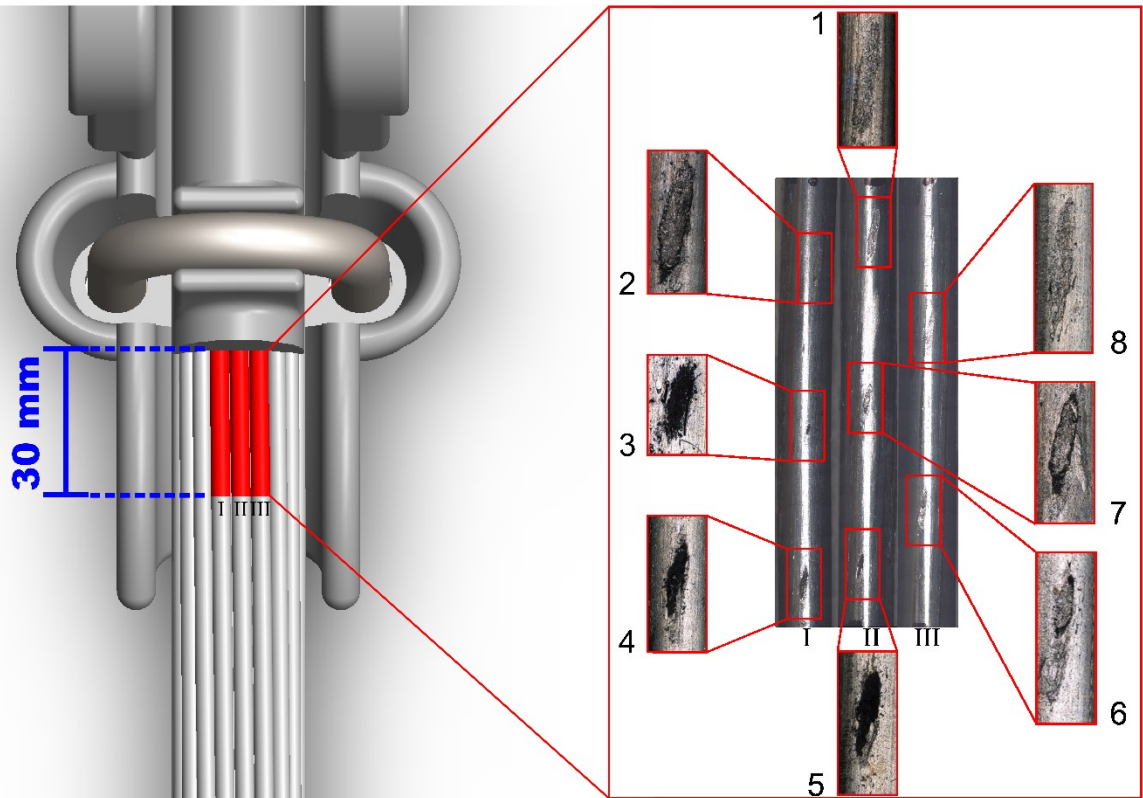



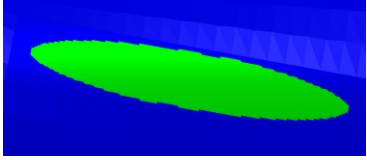

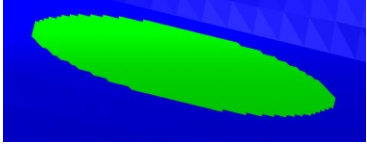

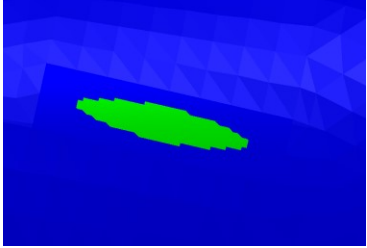
Fig. 3.14. Samples of the three upper wires taken to microscopy analyses, in detail fretting marks between the samples and the inner layer of the AAAC 900 conductor.

The normal contact load estimation was done for all contact marks within the analyzed region, Fig. 3.14. The FE model was generated for each mark based on observed angle α . Results for numerical contact marks that best matched observed mark are shown in Fig. 3.15. Contact marks 2, 6 and 7 are typical fretting fatigue marks characterized by a central stick zone contact and partial slip in surroundings associated with the presence of Al_2O_3 (Azevedo and Cescon, 2002). Contact mark 6 presents also some plastic mark beyond the fretting region, it is argued that parts of the cable moves differently than others during its installation to better accommodate and keep the internal forces balance, in the presence of contact forces it may cause plastic contact marks due to gross slip between wires.

The contact marks 3, 4 and 5 present substantial presence of Al_2O_3 , it evidences gross slip characteristics between layers, such marks are located in the farther region from the keeper, where the stiffness due to clamping is lower and wires can have bigger relative movements.

On the opposite site, the contact marks 1 and 8 have characteristics of static contact marks, these marks are located close to keeper edge, which justifies its features and also presented the biggest marks dimensions.

The loading prediction methodology presented higher mismatch difference between numerical marks and observed marks 3, 4 and 5, it is believed that the massive presence of Al_2O_3 may cause apparent changes in the elliptical shape of the mark, which causes some difficulty to the method to find better fitting of such contact mark.

(a)	a (μm)	b (μm)	α ($^\circ$)	P_{pred} (N)
	1857	289	21	
	1790	299		1267
Percentual Difference (%)	3.6	3.7		
<hr/>				
(b)				
	1274	266	23	
	1348	259		777
Percentual Difference (%)	5.8	2.5		
<hr/>				
(c)				
	479	139	26	
	500	93		101
Percentual Difference (%)	4.3	32.6		

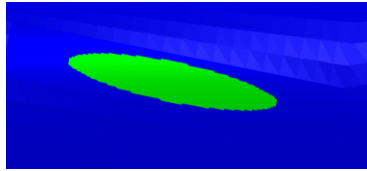
(d)



1154

240

23



1258

240

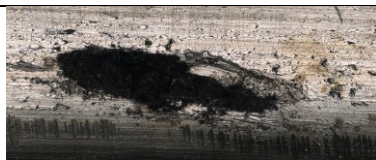
678

Percentual Difference (%)

9.0

0.1

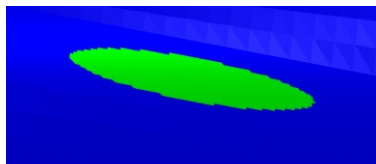
(e)



886

227

26



934

200

421

Percentual Difference (%)

5.5

12.2

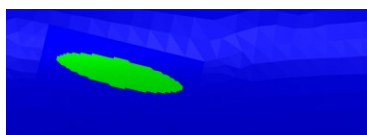
(f)



634

163

27



707

156


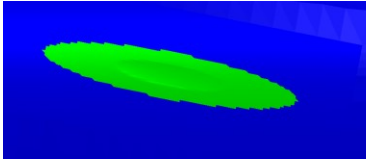
236

Percentual Difference (%)

11.6

3.8

(g)

	1093	212	17
	1095	190	511
Percentual Difference (%)	0.2	-10.4	

(h)


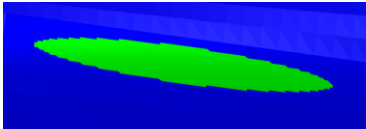
	1505	241	16
	1633	193	699
Percentual Difference (%)	8.5	19.9	

Fig. 3.15. Observed and numerical marks for contact load prediction: (a) contact mark 1, (b) contact mark 2, (c) contact mark 3, (d) contact mark 4, (e) contact mark 5, (f) contact mark 6, (g) contact mark 7 and (h) contact mark 8. (refer to Fig. 3.14)

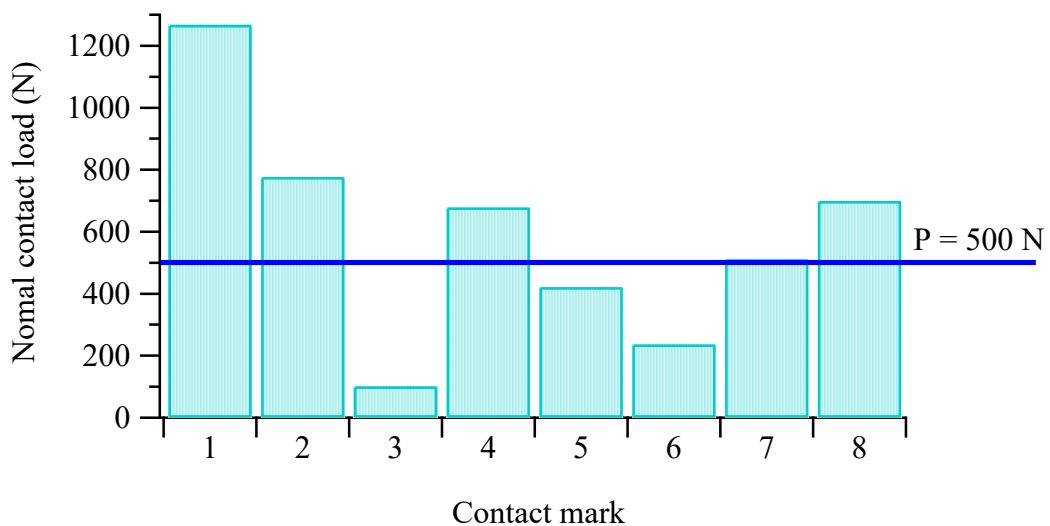


Fig. 3.16. Normal contact load prediction for marks from critical region of the cable.

Figure 3.16 summarizes the contact loads predicted for all contact marks from critical region of the AAAC conductor. The contact marks that presented full adhesion characteristics (marks 1 and 8) have shown an average load equal to 983 N, contact marks in which partial slip characteristics were found (marks 2, 6 and 7) had an average load of 500 N, and gross sliding marks (3, 4 and 5) presented in average 400 N.

3.4 Two contacting wires – preliminary tests

Preliminary fatigue tests on two contacting wires were performed using loading conditions similar to the values found in Section 3.3. The tests were carried out using the experimental apparatus described in Section 3.3.3.2.

The wires were extracted from an AAAC 900 MCM conductor. Similarly to experimental evidence, the crossing angle between wires was chosen 20°. The loading history of each fatigue test was defined as follows: a remote mean load, F_m , was applied to the vertical wire, which was followed by the application of a fixed normal load, P , to the oblique wire; then, the remote load was cycled with a constant amplitude, $\Delta F/2$. The bulk stress amplitude applied to the specimen was equal to 23.7 MPa, while the mean bulk stress varied from 202.4 MPa to 256 MPa. The normal contact load applied to the contacting wires was equal to 500 N, since partial slip characteristics were observed for contact marks presenting around such level of contact load, as shown in Section 3.3.3.3. The loading frequency was chosen around 15 Hz and 20 Hz, failure was defined as complete separation of the specimen and run-out was set at 5×10^6 cycles. The fatigue test data of two contacting wires are summarized in Table 3.3.

Table 3.3. Summary of the fatigue tests of two contacting wires crossed at an angle of 29°.

Specimen ID	D [mm]	P [N]	F_m [N]	$\Delta F/2$ [N]	S_m [MPa]	S_a [MPa]	N_f [cycles]
6201C1	3.96	500	2490	292	202.4	23.7	>5,000,000
6201C2	3.96	500	2490	292	202.4	23.7	>5,000,000
6201C3	3.96	500	2800	292	228.0	23.7	2,844,101
6201C4	3.96	500	3150	292	256.0	23.7	985,499

Table 3.3 reveals that the application of loading conditions similar to the values found by the proposed methodology using the wire-wire test apparatus may result in life ranges close to the full-scale tests carried out on the AAAC 900 conductor (Fig. 3.2).

We aware that this work has limitations, for instance bending effects on the wire and tangential contact load which was not assessed in this study. Such features may explain the lives discrepancy between full-scale tests on the conductor and wire-wire fatigue tests for mean tensile stress equal to 202.4 MPa.

3.5 Conclusions and future work

3.5.1 Conclusions

The present work shows an experimental-numerical methodology for estimating mean tensile load, load amplitude and contact loading between wires of overhead conductors. The loading conditions analysis is done based on study of the region where failures typically occur on the AAAC 900 MCM. The following conclusions can be drawn based on results and analysis presented in this work:

- (1) Full-scale fatigue tests on the AAAC 900 MCM overhead conductor revealed that the majority of wires breaks occurred at the upper part of the outermost layer of the conductor. These failures were found in a distance ahead of the keeper edge ranging from 0.5 to 19 mm, which means that such failures were caused due to the internal contact between wires from subjacent layers.
- (2) Well-controlled tests on single contact wires have shown that a methodology based on simple geometric measurements on contact plastic marks between wires and FE analysis is capable of accurately predicting the normal contact load between wires for several levels of force.
- (3) The static test carried out on the AAAC conductor at a 26.3 kN of tensile load revealed that strains can reach up to 3520 $\mu\text{m}/\text{m}$. It represents 4.57 times the strain of a wire at a free span region of the cable.

- (4) Strain amplitude measurements obtained during the cyclic tests are consistent with the Poffenberger–Swart model. The comparison between strain measurements at the region diametrically opposed to the last point of contact between cable/clamp and measurements beneath the keeper edge revealed slight difference between amplitude strain in such region. Such small difference contrasts with measurements from static test, which shows a fast decay of mean strain according to the distance of strain gages from the keeper edge.
- (5) Assuming uniform stress distribution over the wire cross section, an equivalent mean tensile stress ranging from 53.4 to 242.9 MPa should be applied to a single wire of the AAAC 900 conductor to obtain the same level of axial strain. Regarding the strain amplitude, the equivalent stress amplitude applied to a single wire ranges between 21.8 and 23.7 MPa.
- (6) The methodology for normal contact load determination shows that contact loads drastically change within such small region, the loads can range from 100 N up to 1280 N. For contact marks with partial slip characteristics, the average contact load is around 500 N. Contact marks with full adhesion characteristics presented an average load of 990 N and gross sliding marks an average load of 400 N.
- (7) Preliminary tests on two contacting wires using the wire-wire experimental apparatus resulted in life ranges close to the full-scale tests carried out on the AAAC 900 conductor.

3.5.2 Future Work

Further static and dynamic tests would be done in order to quantify the bending effects on wires located on the critical region of the AAAC 900 conductor. Also, a comparison between features such as fretting zone size and number of cycles to failure would be compared to full-scale tests on the conductor.

References

- Abaqus, 2013. User's Manual and Theory Manual. Hibbit, Karlsson and Sorensen, Inc., Providence, RI, USA.
- Azevedo, C.R.F., Cescon, T., 2002. Failure analysis of aluminum cable steel reinforced (ACSR) conductor of the transmission line crossing the Paraná River. *Eng. Fail. Anal.* 9, 645–664.
- Azevedo, C.R.F., Henriques, A.M.D., Pulino Filho, A.R., Ferreira, J.L.A., Araújo, J.A., 2009. Fretting fatigue in overhead conductors: Rig design and failure analysis of a Grosbeak aluminium cable steel reinforced conductor. *Eng. Fail. Anal.* 16, 136–151.
- Baumann, R., Novak, P., 2017. Efficient computation and experimental validation of ACSR overhead line conductors under tension and bending. *Cigré Science & Engineering* 9, 5–16.
- Badibanga, R. K., 2017. Evaluation of the fatigue resistance of power line conductors function of the h/w parameter. PhD Thesis, University of Brasília.
- Cardou, A., Cloutier, L., Lanteigne, J., M'Boup, P., 1990. Fatigue strength characterization of ACSR electrical conductors at suspension clamps. *Electr. Power Sys. Res.* 19, 61–71.
- Cardou, A., Cloutier, L., M. St-Louis, A. Leblond, 1992. ACSR electrical conductor fretting fatigue at spacer clamps. , in: M. Helmi Attia, R.B. Waterhouse (Eds.), *Standardization of fretting fatigue test methods and equipment (1992)*, 1992, pp. 231–242.
- Cardou, A., Leblond, A., Cloutier, L., 1993. Suspension clamp and ACSR electrical conductor contact conditions. *J. of Energy Eng.* 119, 19–31.
- CIGRÉ, 2007. Fatigue endurance capability of conductor/clamp systems, Task Force B2.11.07.
- Cloutier, L., Goudreau, S., Cardou, A., 2006. Fatigue of overhead conductors. Chapter 3 of EPRI *Transmission Line Reference Book: Wind-Induced Conductor Motion*. Palo Alto, CA.

- Dowling, N.E., Calhoun, C.A., Arcari, A., 2009. Mean stress effects in stress-life fatigue and the Walker equation. *Fatigue Fract. Eng. Mater. Struct.* 32, 163–179.
- Fadel, A.A., Rosa, D., Murça, L.B., Ferreira, J.L.A., Araújo J.A., 2012. Effect of high mean tensile stress on the fretting fatigue life of an Ibis steel reinforced aluminum conductor, *Int. J. Fatigue* 42 24–34.
- Ferguson, J.M., Gibbon, R.R., 1994. Overhead transmission lines – refurbishment and developments. *Power Eng. J.* 8, 109–118.
- Johnson, K.L., 1985. *Contact mechanics*. Cambridge University Press, Cambridge.
- Kaufman, J.G., 2000. *Introduction to aluminum alloys and tempers*. ASM International.
- Lalonde, S., Guilbault, R., Langlois, S., 2018. Numerical analysis of ACSR conductor-clamp systems undergoing wind-induced cyclic loads. *IEEE Transactions on Power Delivery* 33, 1518–1526.
- Lalonde, S., Guilbault, R., Langlois, S., 2018. Numerical analysis of ACSR conductor-clamp systems undergoing wind-induced cyclic loads. *IEEE Transactions on Power Delivery* 33, 1518–1526.
- Lalonde, S., Guilbault, R., Légeron, F., 2017. Modeling multilayered wire strands, a strategy based on 3D finite element beam-to-beam contacts - Part I: Model formulation and validation. *Int. J. Mech. Sci.* 126, 281–296.
- Lévesque, F., Goudreau, S., Cloutier, L., Cardou, A., 2011a. Finite element model of the contact between a vibrating conductor and a suspension clamp. *Tribology International* 44, 1014–1023.
- Lévesque, F., Goudreau, S., Cloutier, L., 2011b. Elastic-plastic microcontact model for elliptical contact areas and its application to a treillis point in overhead electrical conductors. *J. Tribology* 133, 011401-1–011401-9

Lévesque, F., Goudreau, S., Cardou, A., Cloutier, L., 2010. Strain measurements on ACSR conductors during fatigue tests I – Experimental method and data. *IEEE Transactions on Power Delivery*, 25(4), 2825–2834.

Lévesque, F., Légeron, F., 2011. Effect of mean tension on interwire contacts in overhead conductors. Ninth International Symposium on Cable Dynamics, Shanghai, China, 2011.

Neuber, H., 1958. *Theory of notch stresses*. Berlin: Springer.

Ouaki, B., Goudreau, S., Cardou, A., Fiset, M., 2002. Fretting fatigue analysis of aluminium conductor wires near the suspension clamp: metallurgical and fracture mechanics analysis. *J. Strain Analysis* 38, 133–147.

Papailiou, K.O., 1997. On the bending stiffness of transmission line conductors. *IEEE Transactions on Power Delivery*, 12(4), 1576–1588.

Peterson, R.E., 1959. Notch sensitivity. In: *Metal Fatigue*, Edited by Sines, G. and Waisman, J.L., 293–306. McGraw-Hill, New York.

Poffenberger J.C., Swart R.L., 1965. Differential displacement and dynamic conductor strain, *IEEE Trans. Power Appar. Syst.* 84 281–289.

Qi, G., 2013. Computational modeling for stress analysis of overhead transmission line stranded conductors under design and fretting fatigue conditions. PhD Thesis, McGill University

Ruiz C., Boddington P.H.B., Chen K.C., 1984. An investigation of fatigue and fretting in a dovetail joint. *Exp. Mech.* 24, 208–217.

Steier, V.F., Kalombo, R.B., Silva, C.R.M., Nogueira, M.N., Araújo, J.A., 2014. Effect of chromium nitride coatings and cryogenic treatments on wear and fretting fatigue resistance of aluminium. *Electric Power Systems Research* (116), 322–329.

- Susmel, L., Taylor, D., 2007. A novel formulation of the theory of critical distances to estimate lifetime of notched components in the medium-cycle fatigue regime. *Fatigue Fract. Eng. Mater. Struct.* 30, 567–581.
- Susmel, L., 2009. *Multiaxial notch fatigue: From nominal to local stress-stress quantities*. Woodhead, Cambridge, UK.
- Socie, D., 1987. Multiaxial fatigue damage models. *J. Eng. Mater. Technol.* 109, 293–298.
- Smith, K.N., Watson, P., Topper, T.H., 1970. A stress-strain function for the fatigue of metals. *J. Mater.* 5, 767–778.
- Taylor, D., 1999. Geometrical effects in fatigue: a unifying theoretical model. *Int. J. Fatigue* 21, 413–420.
- Taylor, D., 2007. *The theory of critical distances*. Oxford: Elsevier.
- Zhou, Z.R., Cardou, A., Goudreau, S., Fiset, M., 1994a. Fretting patterns in a conductor- clamp contact zone. *Fatigue Fract. Eng. Mater. Struct.* (6), 661–669.
- Zhou, Z.R., Cardou, A., Fiset, M., Goudreau, S., 1994b. Fretting fatigue in electrical transmission lines. *Wear* (173), 179–188.
- Zhou, Z.R., Cardou, A., Goudreau, S., Fiset, M., 1996. Fundamental investigations of electrical conductor fretting fatigue. *Tribol. Int.* (29), 221–232.